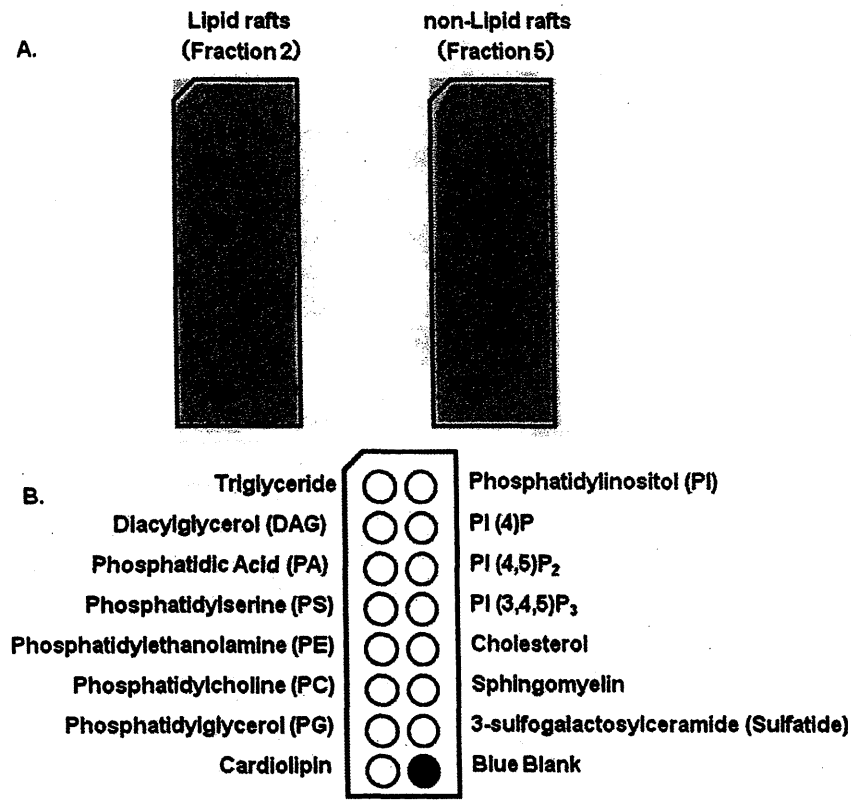

Fig. 5. Interaction of NEP with various lipids. Lipid-attached membrane was treated with sucrose density fractions of SH-SY5Y neuronal cells. After incubation and washing, the membrane was incubated with anti-NEP monoclonal antibody as described in Materials and Methods. The bound NEP was detected by ECL advance. **A:** ECL results. **B:** Lipids attached to the membrane.

Direct Inteaction of NEP With Lipids

The results described above suggest that NEP is localized in lipid rafts, possibly by its direct association with cholesterol. Finally, interaction of NEP with lipids was investigated by using lipid-spotted P-6002 membrane. Fractionated rafts (fraction 2 in Fig. 1A) and non-rafts fractions (fraction 5 in Fig. 1A) were concentrated by ultracentrifugation and incubated with lipids. After washing of the P-6002 membrane, lipid-bound NEP was detected by the specific antibody. Unexpectedly, NEP both in lipid rafts and in nonrafts fractions interacted with phosphatidylserine and cardiolipin but not with cholesterol (Fig. 5).

DISCUSSION

In this study, we found that only the mature form of NEP, glycosylated in the Golgi, and not the immature form, residing in the ER, was localized in lipid rafts (Fig. 1A,B). This indicates that complete glycosylation is required for the association of NEP with lipid rafts. Two possible explanations for this were considered. One is that maturation may be necessary for NEP to bind to a carrier protein such as a glycosylphosphatidylinositol (GPI)-anchored protein. The other is that a small conformational change caused by maturation increases the affinity of NEP for molecules found in lipid rafts, such as sphingolipids and cholesterol. With regard to the former, there have been several reports concerning carrier proteins. One study found that, when the transmembrane and C-terminal domains of BACE1 were replaced with a GPI anchor signal sequence, it was translocated to lipid rafts (Cordy et al., 2003). Another study found that the addition of the N-terminal domain of growth-associated protein 43 (GAP43) to the N-terminus of NEP increased the amount of NEP present in lipid rafts by 1.3-fold (Hama et al., 2004). With regard to the latter possible explanation, we found evidence that the localization of the mature form of NEP in lipid rafts was dependent on the content of cholesterol (Figs. 2, 3). Interestingly, although NEP was completely delocalized by cholesterol depletion, flotillin-1, a lipid raft marker, was not delocalized from lipid rafts by treatment with MβCD (Fig. 2). In this regard, flotillin-1 has been reported to be enriched in detergent-resistant microdomains that are MβCD resistant, although the mechanism

remains to be investigated (Rajendran et al., 2003). Moreover, to examine whether the delocalization of NEP from lipid rafts was caused by its direct association with cholesterol, we extracted lipid raft membranes and treated them with MβCD in vitro (Fig. 3). Consistently with the results presented in Figure 2, NEP was delocalized from lipid rafts membrane by cholesterol depletion, although not completely so (Fig. 3). The difference in the efficiency of NEP delocalization between cell and cell-free systems may be caused by the different conditions used (reaction temperature, membrane state, effects of ultracentrifugation). We conclude that the localization of mature NEP in lipid rafts depends on their cholesterol content.

We investigated the direct association of NEP with pure phospholipids and cholesterol (Fig. 5). Both NEP in rafts and nonrafts directly interacted with phosphatidylserine and cardiolipin. Cardiolipin is a major phospholipid of inner membrane of mammalian mitochondria, so phosphatidylserine might be the major interactor of NEP in lipid rafts. Moreover, immunocytochemical analysis showed that the clustered localization of endogenous NEP in SH-SY5Y cells became dispersed after MβCD treatment (Supp. Info. Fig. 1). Therefore, we conclude that NEP directly associated with phosphatidylserine in cholesterol-rich lipid rafts and MβCD-induced cholesterol depletion triggers the destruction of lipid composition and releases the NEP from rafts. However, the protease activities of mature NEP were unexpectedly comparable in lipid raft and nonlipid raft fractions, as assessed by *p*-NA peptide assay. It is possible that the fractionated lipid rafts did not reflect intracellular conditions (Pike, 2004). However, this result suggests that the association with lipid rafts does not itself modify the protease activity of NEP.

Considering the localization of Aβ in lipid rafts through association with cholesterol (Kakio et al., 2002), we hypothesized that the localization of mature NEP in lipid rafts facilitated its association with Aβ and thereby altered Aβ degradation. Recent studies have shown that lipid raft-dependent endocytosis is the predominant Aβ uptake mechanism (Lai and McLaurin, 2011), that there are correlations between memory deficits and intracellular Aβ levels in several mouse AD models (Billings et al., 2005; Knobloch et al., 2007; Bayer and Wirths, 2008), and that intracellular Aβ level correlates with extracellular amyloid deposition (Yang et al., 2011). Thus, it seems reasonable to conclude that NEP is localized and active in lipid rafts. Indeed, NEP is detected primarily in presynapses and on or around axons in the hippocampal formation (Fukami et al., 2002), and presynaptic NEP efficiently degrades Aβ (Iwata et al., 2004). Considering these findings, together with the fact that the ϵ4 allele of apolipoprotein E (apoE) is a risk factor in nonfamilial AD (Kim et al., 2009), we suggest that cholesterol, overloaded by aging or a high-fat diet, enlarges the area occupied by lipid rafts, thereby decreasing the likelihood of NEP and Aβ coming into contact with each other. As a result, Aβ becomes more abundant, oligomerizes, and causes memory deficits. However, it should be noted that cholesterol itself is a crucial contributor to synaptic structure and function. It has been reported that brain-derived neurotrophic factor (BDNF)-dependent cholesterol biosynthesis plays an important role in synapse development (Suzuki et al., 2007). It would therefore be important to maintain normal cholesterol metabolism during AD therapy.

We further investigated the effects of dimerization on the localization of NEP in lipid rafts. We introduced the E403C mutation into human NEP for the first time. The mutation was originally discovered in rabbit NEP, in which it causes the formation of a covalent homodimer (rabbit NEP normally exists as a monomer). Our results show that human NEP E403C, like rabbit NEP E403C, forms a covalent homodimer. In contrast, human NEP WT, like porcine NEP WT (Kenny et al., 1983), forms a noncovalent homodimer (Fig. 4A,B). Moreover, the noncovalent human NEP WT homodimer, though not resistant to NP-40 or Triton X-100, was resistant to DDM and digitonin. DDM and digitonin dissolve proteins modestly, so the complex remained intact after treatment with these detergents. Interestingly, the localization of mature NEP to lipid rafts was enhanced by its homodimerization (Fig. 4D). With regard to the endopeptidase activity of NEP E403C, Vmax/Km for this mutant was decreased by 50% compared with that for wild-type by using either [D-Ala^2, Leu^5] enkephalin or Suc-Ala-Ala-Leu-NH-Np as a substrate (Hoang et al., 1997). Although the NEP E403C mutant seems to be artificial and to have no physiological significance, these results imply that the protease activity of NEP might be modulated by its dimerization.

In conclusion, we have shown that cholesterol regulates the localization of mature NEP in lipid rafts, where its substrate, Aβ, accumulates. Cholesterol does not, however, modulate the protease activity of NEP.

ACKNOWLEDGMENTS

We thank Dr. Nobuhisa Iwata (Nagasaki University) for providing the protocol for the assay of neprilysin-dependent neutral endopeptidase activity.

REFERENCES

Angelisova P, Drbal K, Horejsi V, Cerny J. 1999. Association of CD10/neutral endopeptidase 24.11 with membrane microdomains rich in glycosylphosphatidylinositol-anchored proteins and Lyn kinase. Blood 93:1437–1439.

Bayer TA, Wirths O. 2008. Review on the APP/PS1KI mouse model: intraneuronal Abeta accumulation triggers axonopathy, neuron loss and working memory impairment. Genes Brain Behav 7(Suppl 1):6–11.

Billings LM, Oddo S, Green KN, McGaugh JL, LaFerla FM. 2005. Intraneuronal Abeta causes the onset of early Alzheimer's disease-related cognitive deficits in transgenic mice. Neuron 45:675–688.

Cordy JM, Hussain I, Dingwall C, Hooper NM, Turner AJ. 2003. Exclusively targeting beta-secretase to lipid rafts by GPI-anchor addition up-regulates beta-site processing of the amyloid precursor protein. Proc Natl Acad Sci U S A 100:11735–11740.

Fukami S, Watanabe K, Iwata N, Haraoka J, Lu B, Gerard NP, Gerard C, Fraser P, Westaway D, St. George-Hyslop P, Saido TC. 2002.

Abeta-degrading endopeptidase, neprilysin, in mouse brain: synaptic and axonal localization inversely correlating with Abeta pathology. Neuroscience research 43:39–56.

Hama E, Shirotani K, Iwata N, Saido TC. 2004. Effects of neprilysin chimeric proteins targeted to subcellular compartments on amyloid beta peptide clearance in primary neurons. J Biol Chem 279:30259–30264.

Hardy JA, Higgins GA. 1992. Alzheimer's disease: the amyloid cascade hypothesis. Science 256:184–185.

Hellstrom-Lindahl E, Ravid R, Nordberg A. 2008. Age-dependent decline of neprilysin in Alzheimer's disease and normal brain: inverse correlation with A beta levels. Neurobiol Aging 29:210–221.

Hoang MV, Sansom CE, Turner AJ. 1997. Mutagenesis of Glu403 to Cys in rabbit neutral endopeptidase-24.11 (neprilysin) creates a disulphide-linked homodimer: analogy with endothelin-converting enzyme. Biochem J 327:925–929.

Iwata N, Tsubuki S, Takaki Y, Shirotani K, Lu B, Gerard NP, Gerard C, Hama E, Lee HJ, Saido TC. 2001. Metabolic regulation of brain Abeta by neprilysin. Science 292:1550–1552.

Iwata N, Takaki Y, Fukami S, Tsubuki S, Saido TC. 2002. Region-specific reduction of A beta-degrading endopeptidase, neprilysin, in mouse hippocampus upon aging. J Neurosci Res 70:493–500.

Iwata N, Mizukami H, Shirotani K, Takaki Y, Muramatsu S, Lu B, Gerard NP, Gerard C, Ozawa K, Saido TC. 2004. Presynaptic localization of neprilysin contributes to efficient clearance of amyloid-beta peptide in mouse brain. J Neurosci 24:991–998.

Kakio A, Nishimoto S, Yanagisawa K, Kozutsumi Y, Matsuzaki K. 2002. Interactions of amyloid beta-protein with various gangliosides in raft-like membranes: importance of GM1 ganglioside-bound form as an endogenous seed for Alzheimer amyloid. Biochemistry 41:7385–7390.

Kanemitsu H, Tomiyama T, Mori H. 2003. Human neprilysin is capable of degrading amyloid beta peptide not only in the monomeric form but also the pathological oligomeric form. Neurosci Lett 350:113–116.

Kawarabayashi T, Shoji M, Younkin LH, Wen-Lang L, Dickson DW, Murakami T, Matsubara E, Abe K, Ashe KH, Younkin SG. 2004. Dimeric amyloid beta protein rapidly accumulates in lipid rafts followed by apolipoprotein E and phosphorylated tau accumulation in the Tg2576 mouse model of Alzheimer's disease. J Neurosci 24:3801–3809.

Kenny AJ, Fulcher IS, McGill KA, Kershaw D. 1983. Proteins of the kidney microvillar membrane. Reconstitution of endopeptidase in liposomes shows that it is a short-stalked protein. Biochem J 211:755–762.

Kim J, Basak JM, Holtzman DM. 2009. The role of apolipoprotein E in Alzheimer's disease. Neuron 63:287–303.

Knobloch M, Konietzko U, Krebs DC, Nitsch RM. 2007. Intracellular Abeta and cognitive deficits precede beta-amyloid deposition in transgenic arcAbeta mice. Neurobiol Aging 28:1297–1306.

Kojro E, Gimpl G, Lammich S, Marz W, Fahrenholz F. 2001. Low cholesterol stimulates the nonamyloidogenic pathway by its effect on the alpha-secretase ADAM 10. Proc Natl Acad Sci U S A 98:5815–5820.

Lafrance MH, Vezina C, Wang Q, Boileau G, Crine P, Lemay G. 1994. Role of glycosylation in transport and enzymic activity of neutral endopeptidase-24.11. Biochem J 302:451–454.

Lai AY, McLaurin J. 2011. Mechanisms of amyloid-beta peptide uptake by neurons: the role of lipid rafts and lipid raft-associated proteins. Int J Alzheimers Dis 2011:548380.

Matsuzaki K, Noguch T, Wakabayashi M, Ikeda K, Okada T, Ohashi Y, Hoshino M, Naiki H. 2007. Inhibitors of amyloid beta-protein aggregation mediated by GM1-containing raft-like membranes. Biochim Biophys Acta 1768:122–130.

Pike LJ. 2004. Lipid rafts: heterogeneity on the high seas. Biochem J 378:281–292.

Pike LJ. 2006. Rafts defined: a report on the Keystone Symposium on Lipid Rafts and Cell Function. J Lipid Res 47:1597–1598.

Rajendran L, Masilamani M, Solomon S, Tikkanen R, Stuermer CA, Plattner H, Illges H. 2003. Asymmetric localization of flotillins/reggies in preassembled platforms confers inherent polarity to hematopoietic cells. Proc Natl Acad Sci U S A 100:8241–8246.

Riemann D, Hansen GH, Niels-Christiansen L, Thorsen E, Immerdal L, Santos AN, Kehlen A, Langner J, Danielsen EM. 2001. Caveolae/lipid rafts in fibroblast-like synoviocytes: ectopeptidase-rich membrane microdomains. Biochem J 354:47–55.

Selkoe DJ. 2002. Alzheimer's disease is a synaptic failure. Science 298:789–791.

Suzuki S, Kiyosue K, Hazama S, Ogura A, Kashihara M, Hara T, Koshimizu H, Kojima M. 2007. Brain-derived neurotrophic factor regulates cholesterol metabolism for synapse development. J Neurosci 27:6417–6427.

von Treskow B, Kallen KJ, von Strandmann EP, Borchmann P, Lange H, Engert A, Hansen HP. 2004. Depletion of cellular cholesterol and lipid rafts increases shedding of CD30. J Immunol 172:4324–4331.

Wada S, Morishima-Kawashima M, Qi Y, Misono H, Shimada Y, Ohno-Iwashita Y, Ihara Y. 2003. Gamma-secretase activity is present in rafts but is not cholesterol-dependent. Biochemistry 42:13977–13986.

Yang DS, Stavrides P, Mohan PS, Kaushik S, Kumar A, Ohno M, Schmidt SD, Wesson D, Bandyopadhyay U, Jiang Y, Pawlik M, Peterhoff CM, Yang AJ, Wilson DA, St. George-Hyslop P, Westaway D, Mathews PM, Levy E, Cuervo AM, Nixon RA. 2011. Reversal of autophagy dysfunction in the TgCRND8 mouse model of Alzheimer's disease ameliorates amyloid pathologies and memory deficits. Brain 134:258–277.

The American Journal of Pathology, Vol. 180, No. 4, April 2012

DOI: 10.1016/j.ajpath.2011.12.040

Molecular Pathogenesis of Genetic and Inherited Diseases

In Vivo Characterization of Mutant Myotilins

Etsuko Keduka,* Yukiko K. Hayashi,* Sherine Shalaby,* Hiroaki Mitsuhashi,*† Satoru Noguchi,* Ikuya Nonaka,* and Ichizo Nishino*

From the Department of Neuromuscular Research, National Institute of Neuroscience, National Center of Neurology and Psychiatry, Tokyo, Japan; and the Division of Genetics,† Children's Hospital Boston, Harvard Medical School, Boston, Massachusetts*

Myofibrillar myopathy (MFM) is a group of disorders that are pathologically defined by the disorganization of the myofibrillar alignment associated with the intracellular accumulation of Z-disk–associated proteins. MFM is caused by mutations in genes encoding Z-disk–associated proteins, including myotilin. Although a number of MFM mutations have been identified, it has been difficult to elucidate the precise roles of the mutant proteins. Here, we present a useful method for the characterization of mutant proteins associated with MFM. Expression of mutant myotilins in mouse tibialis anterior muscle by *in vivo* electroporation recapitulated both the pathological changes and the biochemical characteristics observed in patients with myotilinopathy. In mutant myotilin-expressing muscle fibers, myotilin aggregates and is costained with polyubiquitin, and Z-disk–associated proteins and myofibrillar disorganization were commonly seen. In addition, the expressed S60C mutant myotilin protein displayed marked detergent insolubility in electroporated mouse muscle, similar to that observed in human MFM muscle with the same mutation. Thus, *in vivo* electroporation can be a useful method for evaluating the pathogenicity of mutations identified in MFM. *(Am J Pathol 2012, 180: 1570–1580; DOI: 10.1016/j.ajpath.2011.12.040)*

Myofibrillar myopathy (MFM) is a group of neuromuscular diseases with common morphological features such as disorganized myofibrillar alignment and accumulation of Z-disk–associated proteins.[1] Mutations in genes encoding Z-disk–associated proteins are known to cause MFM. Disease-associated mutations have been identified in six genes, including myotilin, desmin, αB-crystallin, ZASP, filamin C, and BAG3.[2,3] Elucidation of their pathogenicity, however, is sometimes difficult.

Myotilin (myofibrillar protein with titin-like immunoglobulin domains) is a 57-kDa protein with 10 exons encoded by the myotilin gene (*MYOT*) on chromosome 5q31. Myotilin consists of a unique serine-rich domain at the N-terminus and two Ig-like domains at the C-terminus.[4–7] Myotilin is highly expressed in skeletal and cardiac muscle, and localizes to the Z-disk,[4] which plays important roles in sarcomere assembly, actin filament stabilization, and muscle force transmission.[8,9] Myotilin interacts with several Z-disk–associated proteins, including α-actinin,[4] filamin C,[10,11] FATZ,[11] ZASP,[12] and MuRF ubiquitin ligase.[13] Myotilin also interacts with actin monomers and filaments through its Ig-like domains, which also mediate homodimerization.[14] Previous studies have shown that myotilin can bundle actin filaments *in vitro*, acting alone or in collaboration with α-actinin and filamin C.[4,14,15] Thus, myotilin is thought to play a role in anchoring and stabilizing actin filaments at the Z-disk, and is involved in the organization and maintenance of Z-disk integrity.[12] Missense mutations in *MYOT* have been associated with MFM,[16–18] limb girdle muscular dystrophy type 1A,[17,19,20] and distal myopathy.[21,22] We have previously identified a mutation p.Arg405Lys (R405K) in exon 9 in the second Ig-like domain of myotilin. The R405K mutant myotilin exhibited defective homodimerization and decreased interaction with α-actinin in a yeast 2-hybrid (Y2H) system.[23] All of the other previously reported *MYOT* mutations are located in exon 2 [14,16–18,24], with p.Ser60Cys (S60C) being one of the most common mutations. The pathogenic effects of *MYOT* mutations and

Supported by a Grant-in-Aid for Scientific Research from the Japan Society for the Promotion of Science; a Comprehensive Research on Disability Health and Welfare (20B-12, 20B-13) award from the Ministry of Health, Labor and Welfare; a Research on Intractable Diseases award from the Ministry of Health, Labor and Welfare; an Intramural Research Grant (23-4, 23-5, 23-6) for Neurological and Psychiatric Disorders, National Center of Neurology and Psychiatry; and a grant from the Japan Foundation for Neuroscience and Mental Health.

Accepted for publication December 29, 2011.

Supplemental material for this article can be found at *http://ajp.amjpathol.org* or at doi: 10.1016/j.ajpath.2011.12.040.

Address reprint requests to Yukiko K. Hayashi, M.D, Ph.D., Department of Neuromuscular Research, National Institute of Neuroscience, National Center of Neurology and Psychiatry, 4-1-1 Ogawahigashicho, Kodaira, Tokyo, 187-8502, Japan. E-mail: hayasi_y@ncnp.go.jp.

the disease mechanism involved remain poorly understood.

Model animals, such as transgenic mice, have contributed to understanding of the critical pathogenic events in MFM.[25–27] Some MFMs, including myotilinopathies, are late-onset and slowly progressive diseases.[1,3] To reproduce clinical and pathological features in model animals for such late-onset mild myopathy is both labor intensive and time consuming. Among the 10 missense mutations identified to date in patients with myotilinopathy,[14,16–18,23,24] only the Thr57Ile (T57I) mutation reproduces the pathological changes in transgenic mice after 12 months of age.[28] To screen for candidate mutations in MFM, a new method is required for demonstrating the pathogenicity of mutations. In the present study, we expressed mutant myotilin in mouse muscle by *in vivo* electroporation and were able to easily reproduce pathological changes similar to those observed in skeletal muscle from patients with *MYOT* mutations.

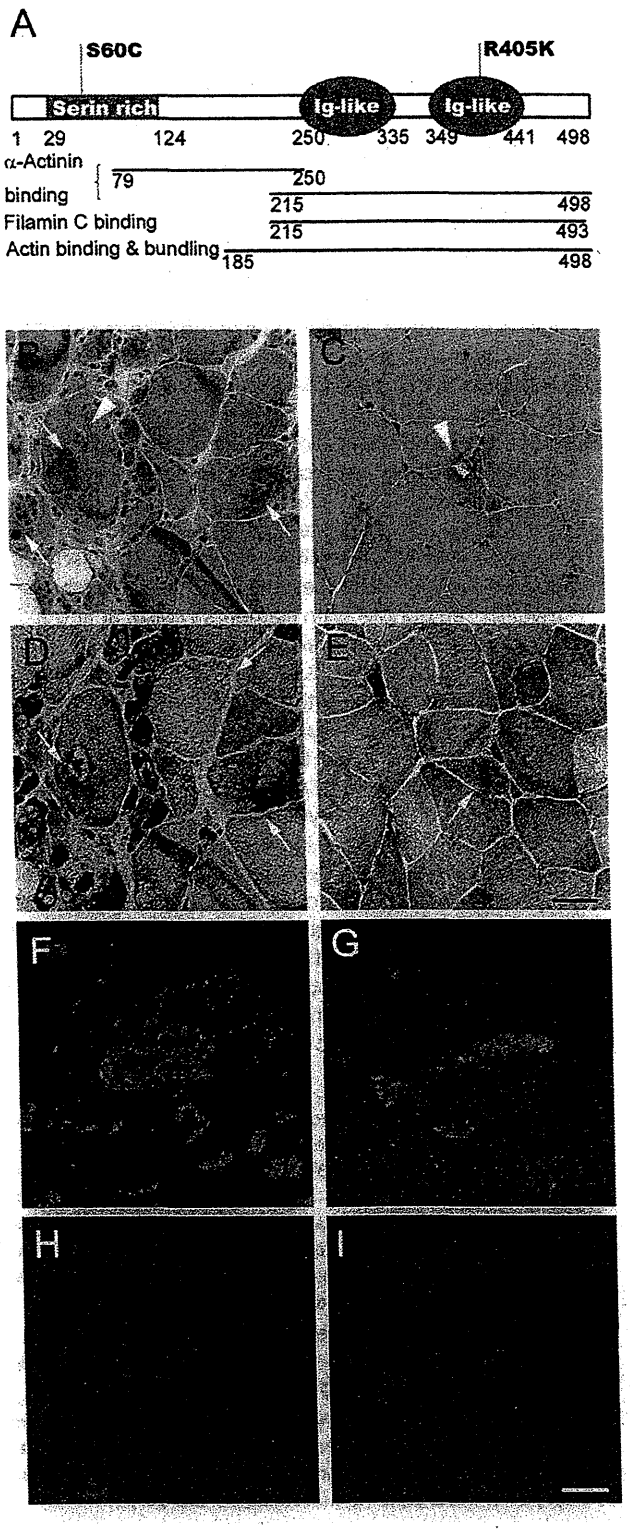

Materials and Methods

Clinical Materials

All clinical materials used in this study were obtained for diagnostic purposes with written informed consent. The studies were approved by the Ethical Committee of the National Center of Neurology and Psychiatry.

Genetic Analysis

Genomic DNA was isolated from peripheral lymphocytes or muscle specimens of patients, using standard techniques. Sequencing and mutation analysis of *MYOT* were performed as described previously.[23]

Plasmid Construction

We cloned full-length human myotilin cDNA and generated mutant myotilin (mMYOT) by site-directed mutagenesis, as described previously.[23] A C→G substitution at nucleotide position 179 and a G→A substitution at nucleotide 1214 were introduced to obtain p.S60C and p.R405K, respectively. A schematic of the location of these mutations in the structure of the myotilin protein is given in Figure 1A. For expression in mammalian cells, cDNAs of wild-type myotilin (wtMYOT) or mMYOT (S60C or R405K) were subcloned into pCMV-Myc vector (Ta-

Figure 1. Myotilin mutations and histopathological findings in myotilinopathy patients. **A:** Myotilin structure and disease-related mutations. p.Ser60Cys (S60C) is located in the serine-rich domain and p.Arg405Lys (R405K) is located in the second immunoglobulin (Ig)-like domain of myotilin. **B–I:** Pathological changes in muscles from patient 1 with *MYOT* S60C (**B**, **D**, **F**, and **H**) and from patient 2 with *MYOT* R405K (**C**, **E**, **G**, and **I**). **B:** Modified Gömöri trichrome (mGT) staining of biopsied skeletal muscle from patient 1 revealed markedly degenerated fibers with many spheroid protein inclusions (**arrows**). Some fibers had rimmed vacuoles (**arrowhead**). **C:** mGT staining of biopsied skeletal muscle from patient 2 revealed scattered fibers with rimmed vacuoles (**arrowhead**). **D:** NADH tetrazolium reductase (NADH-TR) staining of the serial section shown in **B** revealed markedly disorganized intermyofibrillar networks (**arrows**). **E:** NADH-TR staining of the serial section shown in **C** revealed disorganized intermyofibrillar networks (**arrow**). **F–I:** Coimmunostaining of muscles from patients using anti-myotilin (green) and anti-polyubiquitin (red) antibodies. **F:** Large accumulations of myotilin were observed in many fibers in patient 1. **G:** Small accumulations of myotilin were seen in some fibers in patient 2. Myotilin aggregates were positive for polyubiquitin in both patient 1 (**H**) and patient 2 (**I**). Scale bars: 50 μm (**B–E**); 20 μm (**F–I**).

kara Bio, Shiga, Japan). All constructs were verified by sequencing. Primer sequences are available on request.

Cell Culture, Transfection, and Immunocytochemical Analysis

C2C12 murine myoblast cells (American Type Culture Collection, Manassas, VA) were cultured in Dulbecco's modified Eagle's medium (Sigma-Aldrich, St. Louis, MO) supplemented with 10% fetal bovine serum (Invitrogen, Carlsbad, CA) at 37°C in a humidified atmosphere of 5% carbon dioxide. The cells were transiently transfected using FuGENE HD transfection reagent (Roche Diagnostics, Indianapolis, IN), according to the manufacturer's instructions. Forty-eight hours after transfection, the cells were fixed in 4% paraformaldehyde, permeabilized with 0.5% Triton-X 100, and costained with anti-Myc antibody (Sigma-Aldrich) and rhodamine-labeled phalloidin (Wako Pure Chemical Industries, Osaka, Japan) to detect transfected myotilin and actin filaments, respectively, according to standard protocol.[29]

In Vivo *Electroporation*

ICR mice were purchased from CLEA Japan (Fuji, Shizuoka, Japan). Animals were handled in accordance with the guidelines established by the Ethical Review Committee on the Care and Use of Rodents in the National Institute of Neuroscience, National Center of Neurology and Psychiatry. All mouse experiments were approved by the Committee. Five-week-old male ICR mice were anesthetized with diethyl ether, and the tibialis anterior (TA) muscles of mice were injected with 80 μg of purified Myc-tagged myotilin plasmid DNA. wtMYOT was injected to one side of TA muscle and mMYOT (S60C or R405K) was injected to the other side of TA muscle. *In vivo* transfection was performed using a square-wave electroporator (CUY-21SC; Nepa Gene, Ichikawa, Japan). A pair of electrode needles was inserted into the muscle to a depth of 3 mm to encompass the DNA injection sites. Each injected site was administered with three consecutive 50 ms-long pulses at the required voltage (50 to 90 V) to yield a current of 150 mA. After a 1-second interval, three consecutive pulses of the opposite polarity were administered. At 7 or 14 days after electroporation, mice were sacrificed by cervical dislocation, and TA muscles were isolated.

Histochemical and Immunohistochemical Analyses

Biopsied human muscles or electroporated mouse TA muscles were frozen in isopentane cooled in liquid nitrogen. Serial 10-μm cryosections were stained with modified Gömöri trichrome (mGT) and NADH-tetrazolium reductase (NADH-TR) and were subjected to a battery of histochemical methods. Immunohistochemistry was performed on serial 6-μm cryosections, as described previously.[29]

Antibodies

The primary antibodies used in this study were as follows: actin (Kantoukagaku, Tokyo, Japan), α-actinin (Sigma-Aldrich), BAG3 (Abcam, Tokyo, Japan), αB-crystallin (StressGen Biotechnologies, Victoria, BC, Canada), desmin (PROGEN Biotechnik, Heidelberg, Germany), filamin C (kindly provided by A.H. Beggs),[30] c-Myc (Sigma-Aldrich), c-Myc (PROGEN Biotechnik), myotilin (Proteintech Group, Chicago, IL), polyubiquitinated protein (Biomol International-Enzo Life Sciences, Plymouth Meeting, PA), GAPDH (Advanced ImmunoChemical, Long Beach, CA), and horseradish peroxidase-labeled anti-c-Myc antibody (Santa Cruz Biotechnology, Santa Cruz, CA).

Evaluation of Aggregates

Histochemical and immunohistochemical analyses were performed on cryosections of electroporated muscles sectioned at 500-μm intervals. The section containing the highest number of Myc-positive fibers (>100 fibers) was used. Myc-positive granules >1 μm in diameter were defined as aggregates. The Myc-positive fibers containing Myc-positive aggregates were counted among all Myc-positive fibers. Five mice each from the wtMYOT-, mMYOT S60C-, and mMYOT R405K-expressing groups were examined. To compare the number and size of Myc-positive aggregates per fiber, we measured the number and area of Myc-positive aggregates in 30 myofibers from each specimen using ImageJ software version 1.43 (NIH, Bethesda, MD). The results are presented as bar graphs (±SD) and histograms. Fifteen serial sections were immunoblotted to measure the amounts of electroporated Myc-tagged myotilin protein.

Electron Microscopy

For electron microscopy, cryosections (25 μm thick) of biopsied muscle with the S60C mutation (patient 1) were fixed with 2% glutaraldehyde in 100 mmol/L cacodylate buffer for 15 minutes on ice. After a shaking with a mixture of 4% osmium tetroxide, 1.5% lanthanum nitrate, and 200 mmol/L s-collidine for 1 to 2 hours, samples were embedded in epoxy resin. TA muscles of 5-week-old ICR mice were coelectroporated with pEGFP-C1 plasmid (Clontech, Tokyo, Japan), which encodes enhanced green fluorescent protein (EGFP), and with either Myc-wtMYOT or Myc-mMYOT (S60C or R405K) plasmid (40 μg each). As a control, pEGFP-C1 plasmid was electroporated alone. TA muscles were isolated 7 and 14 days after electroporation. EGFP-positive regions were trimmed under a fluorescence microscope and fixed with 2% glutaraldehyde in 100 mmol/L cacodylate buffer for 3 hours. After a shaking with a mixture of 4% osmium tetroxide, 1.5% lanthanum nitrate, and 200 mmol/L s-collidine for 2 to 3 hours, samples were embedded in epoxy resin. Semithin sections (1 μm thick) were stained with Toluidine Blue. Ultrathin sections (100 nm thick) were stained with uranyl acetate and lead citrate, and were analyzed at 120 kV using a Tecnai Spirit transmission electron microscope (FEI, Hillsboro, OR).

Solubility and Immunoblot Assay

To examine solubility of mutant myotilin, we used frozen biopsied muscles from human control subjects and from the two myotilinopathy patients, as well as TA muscles of six mice each from the wtMYOT-, mMYOT S60C-, and mMYOT R405K-expressing groups, at 14 days after electroporation. The 1.25-mm^3 specimens of muscle were lysed and homogenized in 150 μL of radioimmunoprecipitation assay buffer containing 50 mmol/L Tris-HCl (pH 7.5), 150 mmol/L NaCl, 1 mmol/L EDTA (pH 8.0), 1% Nonidet P-40, 0.5% sodium deoxycholate, 0.1% SDS, and Roche complete protease inhibitor cocktail (Roche Diagnostics). The lysates were incubated at 4°C for 20 minutes with gentle rotation, and then centrifuged at 15,000 × *g* at 4°C for 20 minutes. The supernatants and precipitates were collected, and the protein concentrations of the supernatants were determined using a protein assay kit (Bio-Rad Laboratories, Hercules, CA). Immunoblotting of the supernatant (detergent-soluble) and precipitate (detergent-insoluble) fractions was performed, as described previously.[23] Glyceraldehyde 3-phosphate dehydrogenase (GAPDH) was used as an internal standard. Immunoreactive complexes on the membranes were detected using enhanced chemiluminescence ECL Plus detection reagent (GE Healthcare, Chalfont St Giles, UK). Insolubility index was calculated as the ratio of the quantity of insoluble protein to the total quantity of proteins (the sum of soluble and insoluble proteins).

Immunoprecipitation

The 5-mm^3 specimens of frozen electroporated mouse muscles isolated at 14 days after electroporation were lysed and homogenized in 0.6 mL of radioimmunoprecipitation assay buffer. The lysates were incubated at 4°C for 20 minutes with gentle rotation, and then centrifuged at 15,000 × *g* at 4°C for 20 minutes. The supernatants were collected, and their protein concentrations were adjusted using a protein assay kit (Bio-Rad Laboratories). Immunoprecipitation was performed as described previously,[23] with agarose-conjugated anti-Myc antibody (Santa Cruz Biotechnology).

Statistical Analysis

Differences between wtMYOT-, mMYOT S60C-, and mMYOT R405K-expressing mice were analyzed with GraphPad Prism version 5 (GraphPad Software, La Jolla, CA). Comparisons among groups were performed by one-way analysis of variance with post hoc Tukey's analysis. Data are expressed as means ± SD.

Results

Mutation Screening and Histochemical Analyses of Muscles from Patients

We performed *MYOT* mutation screening in MFM patients and identified two patients with mutations. Patient 1, harboring a *MYOT* c.179C→G (p.S60C) mutation in exon 2, was a 63-year-old woman with a 6-year-long history of slowly progressive limb muscle weakness. Her mother (deceased) had had muscle weakness. The patient had difficulty in climbing stairs without support, and could not walk for long distances. Her serum creatine kinase level was elevated to 734 IU/L (reference, <200 IU/L). A biopsied specimen from the rectus femoris muscle showed marked variation in fiber size, with some necrotic fibers. Clusters of degenerated fibers with abnormal cytoplasmic inclusions were observed; some fibers with rimmed vacuoles were also seen (Figure 1B). Intermyofibrillar networks were markedly disorganized (Figure 1D). Under electron microscopy, electron-dense materials and cytoplasmic amorphous inclusions of various sizes were seen in some fibers (see Supplemental Figure S1 at *http://ajp.amjpathol.org*). Patient 2 was a 57-year-old woman harboring a *MYOT* c.1214G→A (p.R405K) mutation in exon 9. Detailed clinical symptoms have been described previously.[23] In brief, this patient had a 16-year-long history of slowly progressive proximal limb muscle weakness. Her serum creatine kinase level was mildly elevated (385 IU/l). A specimen from the vastus lateralis muscle showed marked variation in fiber size, scattered fibers with internal nuclei, and small angular fibers. Some fibers with rimmed vacuoles were seen (Figure 1C), and intermyofibrillar networks were disorganized (Figure 1E). Immunohistochemical analysis of muscle specimens from both patients revealed scattered fibers with strong immunoreactive accumulations of myotilin (Figure 1, F and G), which costained with polyubiquitin (Figure 1, H and I), α-B crystallin, BAG3, actin, desmin, and filamin C (see Supplemental Figure S2 at *http://ajp.amjpathol.org*).

Mutant Myotilin Does Not Aggregate in Cultured Cells

To examine the aggregation of mutant myotilins in cultured cells, C2C12 murine myoblasts were transfected with Myc-tagged wtMYOT (Myc-wtMYOT) or Myc-tagged mMYOT (Myc-mMYOT S60C or R405K). After 48 hours, immunostaining with anti-Myc antibody and rhodamine-labeled phalloidin revealed that the expressed Myc-wtMYOT, Myc-mMYOT S60C, and Myc-mMYOT R405K did not form abnormal protein aggregations, and they localized at actin stress fibers (Figure 2). Expression of mMYOT did not affect differentiation of C2C12 cells (data not shown).

Accumulation of Myotilin after Electroporation

To investigate the roles of mutant myotilin, we performed *in vivo* electroporation to express Myc-wtMYOT or Myc-mMYOT (S60C or R405K) in mouse TA muscles. At 7 and 14 days after electroporation, Myc-positive granules with diameters >1 μm were observed in Myc-tagged myotilin-expressing myofibers (Figure 3A). Compared with wtMYOT-expressing myofibers, mMYOT-expressing myofi-

Figure 2. Expression of mutant myotilin in cultured cells. Immunofluorescence staining of transfected Myc-wtMYOT (**A**), Myc-mMYOT S60C (**B**), and Myc-mMYOT R405K (**C**) in C2C12 murine myoblasts. Merged images of Myc-tagged myotilin-expressing cells (green) costained for actin stress fibers (red), and nuclear staining with DAPI (blue). C2C12 myoblasts expressing mMYOT S60C (**B**) or R405K (**C**) did not exhibit protein aggregates, and the mutant myotilin colocalized with actin stress fibers similar to wtMYOT (**A**). Scale bar = 20 μm.

bers contained more granular aggregates that were larger in size. At 7 days after electroporation, Myc-positive aggregates of wtMYOT, mMYOT S60C, and mMYOT R405K were observed in 14 ± 5%, 44 ± 7%, and 21 ± 4% of muscle fibers, respectively (Figure 3B). At 14 days after electroporation, the number of the fibers with aggregates increased to 22 ± 4% in wtMYOT, 50 ± 2% in mMYOT S60C, and 37 ± 3% in mMYOT R405K (Figure 3C). The number and size of Myc-positive aggregates in 30 randomly selected Myc-positive muscle fibers were much higher in mMYOT S60C and slightly higher in mMYOT R405K at 14 days after electroporation than at 7 days (see Supplemental Figure S3 at *http://ajp.amjpathol.org*). These data indicate that the expressed mutant myotilins, and mMYOT S60C in particular, are prone to aggregate in skeletal muscles. The amounts of expressed Myc-tagged myotilin proteins were approximately equal, as measured by immunoblotting (Figure 3D).

Myofibril Disorganization and Z-Disk Streaming in Muscles Expressing Mutant Myotilins

To investigate the ultrastructural characteristics of mutant myotilin-electroporated muscles, we performed electron microscopy at 7 and 14 days after electroporation. In Toluidine Blue-stained longitudinal semithin sections, partial disorganization of the Z-disk was observed in both mMYOT S60C-expressing and mMYOT R405K-expressing TA muscles, but not in control or wtMYOT electroporated muscles (data not shown). Electron microscopy also revealed myofibril disorganization with disrupted Z-disk, such as Z-disk streaming and broadening, in mMYOT-expressing muscles (Figure 4, A and D). Variable-sized (1 to 8 μm in diameter) electron-dense material, with electron densities similar to that of the Z-disk, were also seen in mMYOT-expressing mouse muscles (Figure 4, B and E). The inclusions were occasionally associated with autophagic vacuoles (Figure 4, C and F). These ultrastructural findings were commonly observed in both mMYOT S60C- and mMYOT R405K-expressing mouse muscles.

Mutant Myotilin Aggregates Colocalize with Polyubiquitin and Other Z-Disk–Associated Proteins

To compare the protein accumulations in human and mouse muscles, we performed immunohistochemical analysis. At 14 days after electroporation, some cytoplasmic inclusions were observed in mGT-stained sections of mMYOT-expressing muscles (Figure 5, A and B). Immunostaining of serial sections revealed that the inclusions were immunopositive for the Myc tag (Figure 5, A and B). The aggregates of Myc-mMYOT (S60C and R405K) strongly colocalized with polyubiquitin and αB-crystallin. Accumulations of other Z-disk–associated proteins were also observed, including BAG3, actin, desmin, and filamin C (Figure 5). These findings are similar to the observations made in the patients' muscles (Figure 1, F–I; see also Supplemental Figure S2 at *http://ajp.amjpathol.org*). In the electroporated muscles, Myc-wtMYOT aggregates also colocalized with Z-disk–associated proteins, including αB-crystallin, BAG3, actin, desmin, and filamin C (data not shown), whereas only few wtMYOT aggregates were immunopositive for polyubiquitin (Figure 6A).

Mutant Myotilin Proteins Display Marked Detergent Insolubility with Polyubiquitinated Proteins

In the muscle specimens of the two myotilinopathy patients, myotilin aggregates exhibited positive staining for polyubiquitin (Figure 1; see also Supplemental Figure S3 at *http://ajp.amjpathol.org*). Similarly, in electroporated mouse muscles, mMYOT aggregates were positive for polyubiquitin, and polyubiquitin-positive aggregates were more prominently observed in mMYOT S60C-expressing muscles at 14 days after electroporation. On the other hand, only few aggregates of Myc-wtMYOT were positive for polyubiquitin (Figure 6A). This result suggests that mutant myotilin was ubiquitinated or that the expressed mutant myotilin induced the deposition of polyubiquitinated proteins in the muscles of patients and electroporated mice. To characterize these aggregates, we performed a solubility assay. The muscle

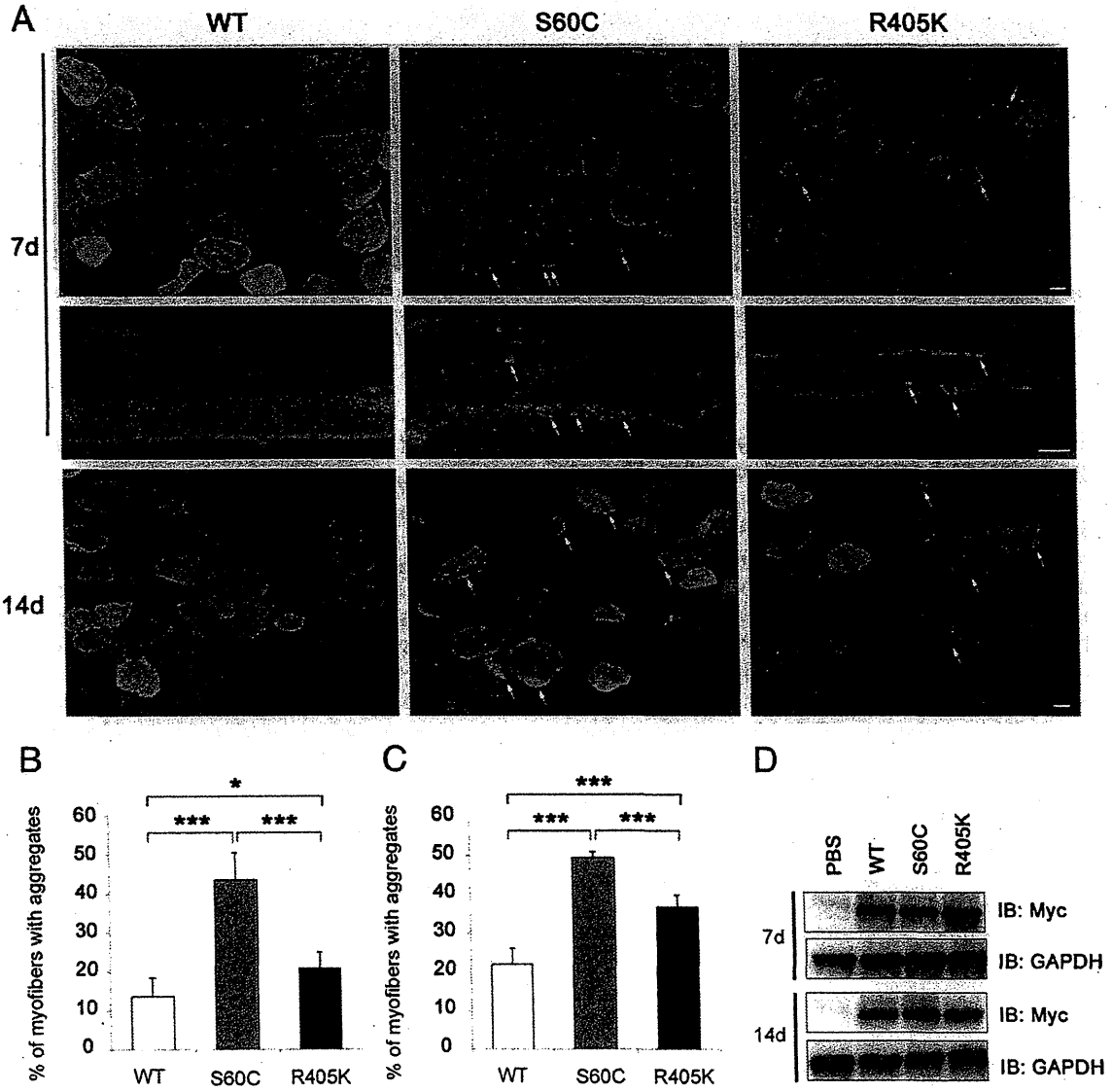

Figure 3. Enhanced aggregation of mutant myotilins in mouse skeletal muscle. **A:** Immunohistochemical staining of Myc-wtMYOT (WT)-electroporated or Myc-mMYOT (S60C or R405K)-electroporated mouse TA muscles. At 7 and 14 days after electroporation, S60C and R405K formed many Myc-positive granular aggregates (**arrows**) in myofibers, compared with WT. More prominent protein aggregates were observed in the S60C-electroporated muscle. At 14 days after electroporation, S60C-expressing myofibers exhibited larger aggregates. Scale bars: 20 μm. **B** and **C:** The percentage of myofibers with Myc-positive aggregates in the electroporated fibers of the WT, S60C, and R405K expression groups (n = 5 mice per group). $^{*}P < 0.05$; $^{***}P < 0.001$. **D:** Immunoblotting analysis of transfected Myc-tagged myotilin in 15 serial sections taken after the sections used for immunohistochemistry. GAPDH was used as a loading control.

specimen with the S60C mutation (patient 1) exhibited increased amounts of myotilin in the detergent-insoluble fraction, compared with the control specimens (Figure 6, B and D). Increasing amounts of polyubiquitinated proteins and αB-crystallin were also detected in the insoluble fraction. On the other hand, the solubilities of myotilin and other proteins, including polyubiquitin, in the muscle specimen with the R405K mutation (patient 2) were similar to those of controls (Figure 6B). Consistently, in the mouse muscles isolated at 14 days after electroporation, markedly increasing amounts of insoluble mMYOT S60C were observed (Figure 6C). In the PBS-injected control muscle, insolubility of endogenous myotilin was 31 ± 12%, whereas in the wtMYOT-, mMYOT S60C-, and mMYOT R405K-injected muscles, the Myc-tagged myotilin amounts in the insoluble fraction were 34 ± 10%, 69 ± 5%, and 48 ± 9%, respectively (Figure 6E). Insolubility of Myc-wtMYOT was similar to that of endogenous myotilin, but mMYOT, and S60C in particular, exhibited higher insolubility (Figure 6E).

These results are consistent with the number of intracellular aggregates observed after electroporation. The amount of polyubiquitinated proteins was markedly increased in the insoluble fraction of mMYOT S60C-electroporated muscles, similar to that of the muscle with the S60C mutation (patient 1) (Figure 6, B and C). A slight increase in the amount of detergent-insoluble polyubiquitinated proteins was observed in mMYOT R405K-electroporated muscles (Figure 6C). The amounts of other

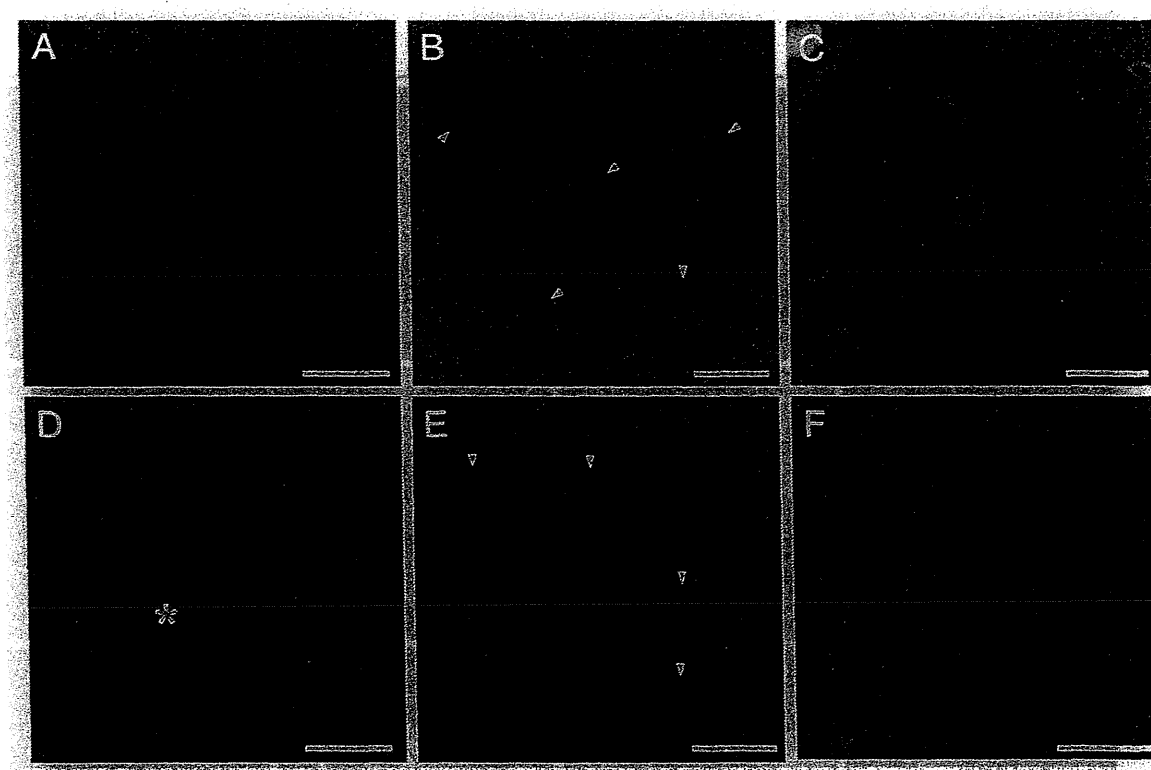

Figure 4. Electron microscopy of muscles expressing mutant myotilin: mMYOT S60C (**A–C**); mMYOT R405K (**D–F**). **A** and **D:** mMYOT-transfected muscle fibers exhibited myofibril disorganization with disrupted Z-disk; note broadening of Z-disks (**A**, **brackets**) and Z-disk streaming (**D**, **asterisk**). **B** and **E:** Variable-sized (1 to 8 μm in diameter) electron-dense inclusions (**arrowheads**) were seen in mMYOT-expressing muscles. **C** and **F:** Inclusions were occasionally associated with autophagic vacuoles (AV). **B** and **C:** Seven days after electroporation. **A** and **D–F:** Fourteen days after electroporation. Scale bars: 3.0 μm (**B** and **E**); 2.0 μm (**C**); 1.7 μm (**A** and **D**); 1.4 μm (**F**).

Z-disk–associated proteins, including αB-crystallin, in the insoluble fraction did not exhibit an increase, even in mMYOT S60C-electroporated muscles (Figure 6C; see also Supplemental Figure S4, A and B, at *http://ajp.amjpathol.org*). We also performed an immunoprecipitation assay to examine whether myotilin was polyubiquitinated. Myc-tagged myotilin proteins were immunoprecipitated from the detergent-soluble fraction of the mouse muscles isolated at 14 days after electroporation. Polyubiquitin immunoreactivity was not detected in the immunoprecipitated proteins (see Supplemental Figure S4C at *http://ajp.amjpathol.org*), indicating that neither the wt-MYOT nor the mMYOT proteins in the soluble fraction were polyubiquitinated.

Discussion

Patients with MFM, including myotilinopathy, exhibit variable clinical features. Some patients exhibit progressive weakness in proximal muscles, whereas others exhibit distal dominant muscle involvement. Cardiomyopathy, peripheral neuropathy, and respiratory insufficiency may be observed.[2] The diagnosis of MFM is generically based on characteristic pathological findings in biopsied muscles, namely, myofibrillar degradation and protein aggregation.[1] Histochemically, the most remarkable pathological changes were observed with mGT staining (Figure 1). Abnormal protein aggregates were observed, including amorphous, granular, or hyaline deposits of various sizes, shapes, and colors (dark blue, blue red, or dark green). The presence of rimmed and nonrimmed vacuoles was also a characteristic observation. Furthermore, NADH-TR staining revealed intermyofibrillar network disorganization. Attenuation or absence of NADH-TR activity in focal areas of myofibers is also observed in MFM.[1,31]

Here, we have presented findings for myotilinopathy patients with similar clinical features but different pathological changes. Fibers with cytoplasmic inclusions and disorganized myofibrils were prominent in the patient with S60C mutation, and these inclusions were strongly immunoreactive for myotilin (Figure 1).

Although transfected cultured cells did not show aggregations, our *in vivo* expression studies in mice were able to reproduce the pathological changes observed in myotilinopathy patients. Mutant myotilin caused enhanced protein aggregation in TA muscles within 1 to 2 weeks (Figure 3). The dark blue or dark green inclusions stained by mGT in mutant-expressing fibers (Figure 4) were similar to those observed in the myotilinopathy patients. Furthermore, mMYOT S60C-expressing myofibers exhibited a greater number of aggregates, which is consistent with the pathology of the patient with that mutation (patient 1). Of note, the size of mMYOT S60C aggregates markedly increased over time, suggesting that mutant myotilin may be resistant to protein degra-

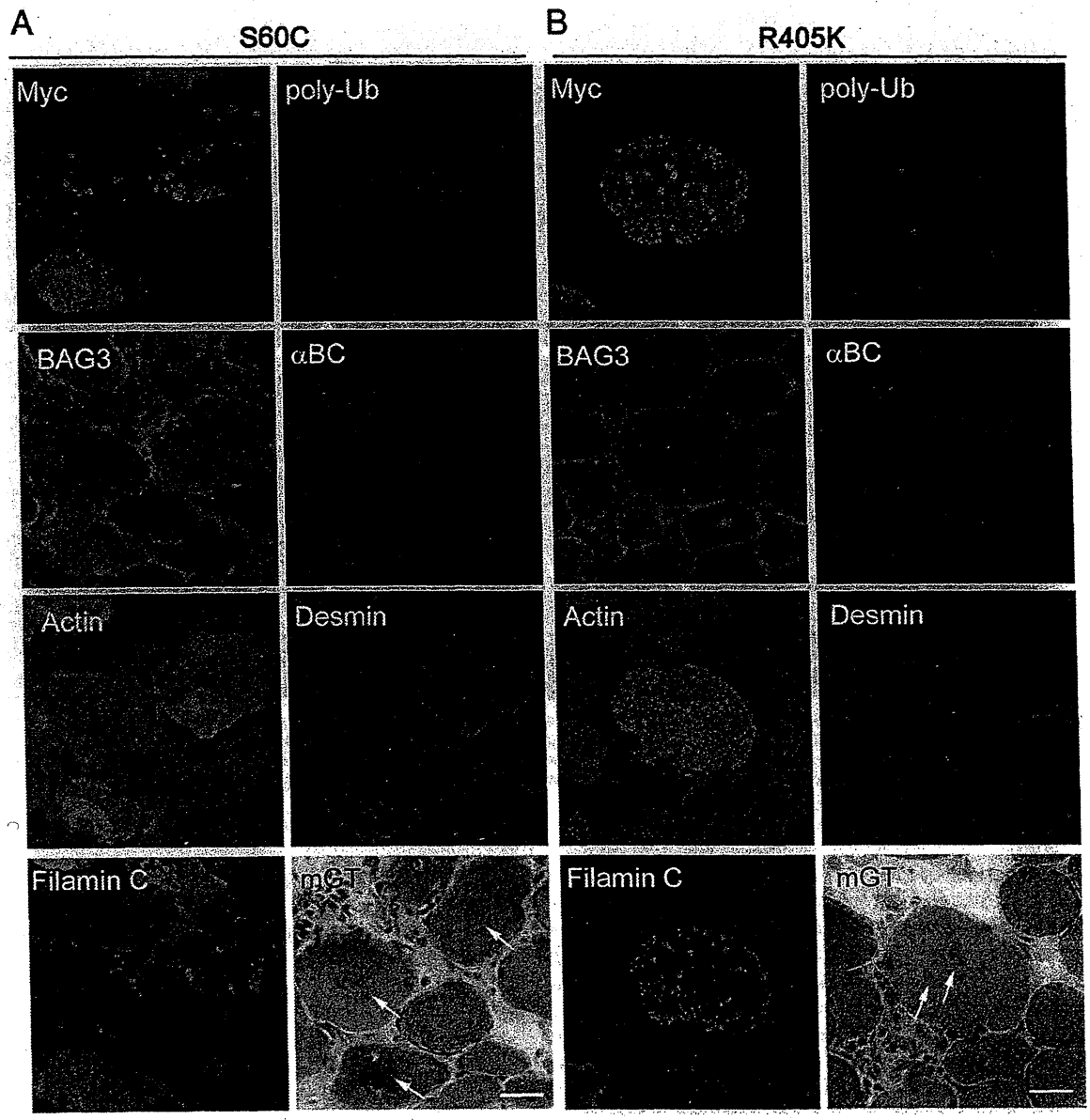

Figure 5. Mutant myotilin aggregates colocalize with polyubiquitin and other Z-disk–associated proteins in electroporated mouse muscle. mGT and immunohistochemical staining of mouse muscle expressing Myc-mMYOT S60C (**A**) or mMYOT R405K (**B**) at 14 days after electroporation. On mGT-stained sections of mMYOT-expressing muscles, cytoplasmic inclusions (**arrows**) were seen. The inclusions were immunopositive for the Myc tag in serial sections. The Myc-positive aggregates of S60C and R405K strongly colocalized with polyubiquitin (poly-Ub) and αB-crystallin (αBC). The aggregates were also immunopositive for BAG3, actin, desmin, and filamin C. Scale bars: 20 μm (**A** and **B**).

dation, as described previously for MFM-associated mutant desmin.[32,33]

Focal disorganization of myofibrils, Z-disk streaming, and accumulation of electron-dense material near the Z-disk are characteristic electron microscopic findings in the muscles of MFM patients.[17,34,35] In the myotilinopathy patient, Z-disk streaming, numerous autophagic vacuoles[17] and cytoplasmic amorphous inclusions were observed (see Supplemental Figure S2 at *http://ajp.amjpathol.org*). In the present study, expression of mMYOT by electroporation elicited myofibril disorganization and accumulation of electron-dense material, which are ultrastructural hallmarks of MFM (Figure 5). Autophagic vacuoles associated with inclusions were also observed in electroporated muscles. Disorganization of myofibrils starting from the Z-disk and material appearing to originate from the Z-disk are commonly observed in MFM patients,[34,35] and these features were also observed in the mMYOT-electroporated muscles. These morphological findings imply that the presence of mutant myotilin can induce characteristic pathological features by affecting Z-disk structure.

Ectopic accumulations of multiple proteins, including Z-disk–associated proteins, are typical pathological features of MFM.[36,37] This study and previous reports[23,38] showed that myotilin-positive protein aggregates colocal-

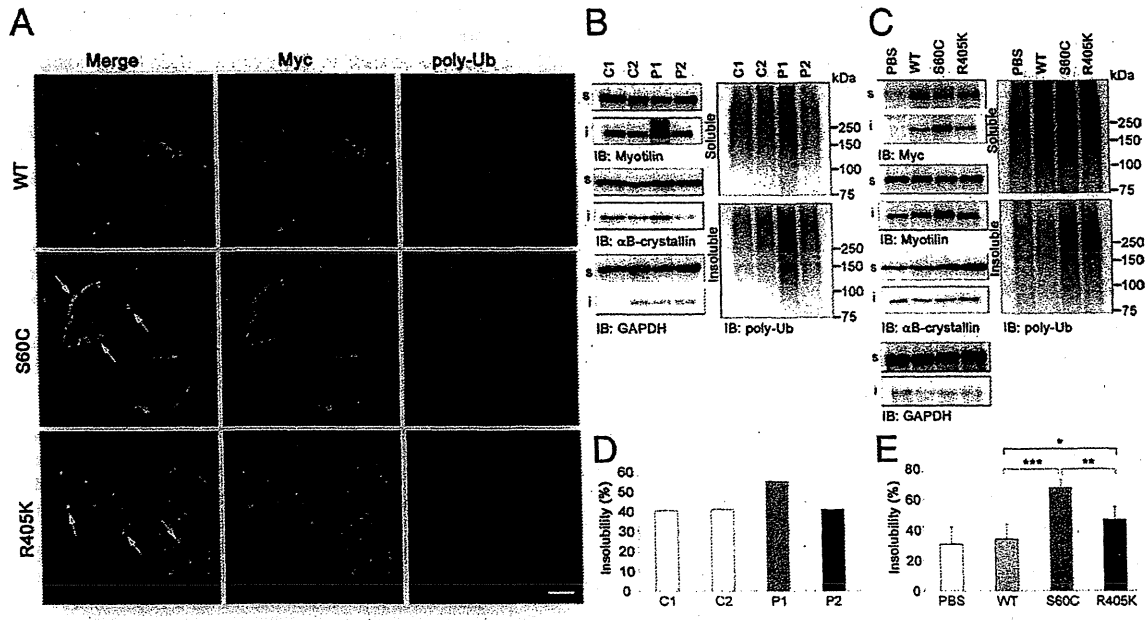

Figure 6. Mutant myotilin displays marked detergent insolubility, along with polyubiquitinated proteins. **A:** At 14 days after electroporation of Myc-wtMYOT (WT) or Myc-mMYOT (S60C or R405K), Myc-mMYOT aggregates, particularly those of S60C, colocalized with polyubiquitin (polyUb) (**arrows**). The WT aggregates rarely costained with polyubiquitin. **B–E** Solubilities of myotilin, polyubiquitinated proteins, and other sarcomeric proteins in muscles from myotilinopathy patients (**B** and **D**) and from electroporated mice (**C** and **E**). GAPDH was used as a loading control. **B:** Immunoblotting of detergent-soluble and detergent-insoluble fractions of muscles from control subjects (C1 and C2) or myotilinopathy patients [P1 (patient 1) and P2 (patient 2)]. In the muscles from P1 with S60C, markedly increasing amounts of myotilin, polyubiquitinated proteins, and αB-crystallin were detected in the insoluble fraction, compared with muscles from control subjects. **D:** Quantification of myotilin insolubilities revealed highest insolubility in P1. **C:** Immunoblotting of detergent-soluble and detergent-insoluble fractions of WT, S60C, or R405K-expressing muscles at 14 days after electroporation. Increasing amounts of insoluble Myc-tagged myotilin proteins and polyubiquitinated proteins were observed in mMYOT-electroporated muscles, compared with WT. Particularly in S60C-electroporated muscles, the amounts of insoluble proteins were notably increased. **E:** Quantification of the insolubilities of electroporated Myc-tagged myotilin in the WT, S60C, and R405K expression groups (n = 6 mice per group). Insolubility of endogenous myotilin was measured using PBS-treated mouse muscles. Compared with WT, insolubilities of electroporated Myc-tagged myotilin were significantly increased in S60C and R405K. $^{*}P < 0.05$; $^{**}P < 0.01$; $^{***}P < 0.001$. Scale bar = 20 μm.

ize with ubiquitin and Z-disk–associated proteins (ie, αB-crystallin, BAG3, actin, desmin, and filamin C) in the muscles of myotilinopathy patients (Figure 1; see also Supplemental Figure S2 at *http://ajp.amjpathol.org*). It has been reported that the myotilin T57I transgenic mice develop progressive myofibrillar changes, including Z-disk streaming and accumulation of mutant myotilin with ubiquitin and Z-disk–associated proteins, similar to those observed in myotilinopathy patients.[28] Expression of mMYOT elicited similar cytoplasmic aggregations in mouse skeletal muscle, and within 2 weeks the aggregates colocalized with polyubiquitin and other Z-disk–associated proteins. Our results indicate that mutant myotilin is able to nucleate aggregations of Z-disk–associated proteins in skeletal muscle.

MFM is a proteinopathy (ie, a protein accumulation disease). In these diseases, protein aggregates are operationally defined by poor solubility in aqueous or detergent solvents.[39,40] Such insoluble protein aggregations are characteristic of many neurodegenerative diseases.[41] In the present study, we discovered that the mutant myotilin S60C protein, along with polyubiquitinated proteins, exhibited marked detergent insolubility in muscles from both the patient and electroporated mice. Mutant myotilin R405K protein showed increased, but lower, detergent insolubility in mice (Figure 6), which may be consistent with the observation that the muscle from the patient with the R405K mutation exhibited only mild protein aggregation (Figure 1). The different detergent insolubilities exhibited by the two *MYOT* mutations may closely correlate with the amounts of protein aggregation. Here, we confirmed the aggregation-prone property of mutant myotilin, which participates in the pathogenesis of myotilinopathy. Using an immunoprecipitation assay, we also showed that electroporated mMYOT was not ubiquitinated in the detergent-soluble fraction (see Supplemental Figure S4 at *http://ajp.amjpathol.org*). A previous study showed that transfected myotilin is degraded by the proteasome system in cultured cells.[42] Our present findings show that ubiquitinated mutant myotilin can form insoluble aggregates. It is also possible that aggregation of insoluble ubiquitinated proteins is induced by the expression of mutant myotilin.

Several causative genes have been identified for MFM; however, in previous studies no mutations were found in nearly half of the MFM patients.[2] To identify the unknown causative genes, easy methods are required for determining the pathogenicity of novel mutations. Some mutant proteins exhibit protein aggregation[43–45] or biological dysfunction, including protein-protein interaction *in vitro*.[23,46–48] However, we could not detect any protein aggregation in mMYOT-expressing cultured cells (Figure 2). The difficulty of *in vitro* investigation may be responsible for the inability to identify Z-disk–associated proteins or mature Z-disk structures. Indeed, myotilin is expressed in later differentiated C2C12 myotubes with

sarcomere-like structures.[49] This suggests that mutant myotilin requires mature Z-disk and/or other sarcomeric proteins to cause aggregations. In such cases, *in vivo* examination is important for evaluating the pathogenicity of mutations. Because *in vivo* electroporation can reproduce the pathological changes observed in MFM patients within a short time, it is a useful and powerful tool for evaluating the pathogenicity of mutations in MFM.

Acknowledgments

We thank Dr. Alan H. Beggs (Children's Hospital Boston, Harvard Medical School) for the kind gift of anti-filamin C antibody and Dr. Satomi Mitsuhashi (Children's Hospital Boston, Harvard Medical School) for technical assistance in electron microscopy analysis.

References

1. Selcen D: Myofibrillar myopathies. Neuromuscul Disord 2011, 21: 161–171
2. Selcen D, Engel AG: Myofibrillar myopathy. (Updated) In GeneReviews. Copyright University of Washington, Seattle. 1997–2012. Available at http://www.ncbi.nlm.nih.gov/books/NBK1499, last revised July 27, 2010
3. OlivÉ M, Odgerel Z, Martínez A, Poza JJ, Bragado FG, Zabalza RJ, Jericó I, Gonzalez-Mera L, Shatunov A, Lee HS, Armstrong J, Maravi E, Arroyo MR, Pascual-Calvet J, Navarro C, Paradas C, Huerta M, Marquez F, Rivas EG, Pou A, Ferrer I, Goldfarb LG: Clinical and myopathological evaluation of early- and late-onset subtypes of myofibrillar myopathy. Neuromuscul Disord 2011, 21:533–542
4. Salmikangas P, Mykkänen OM, Grönholm M, Heiska L, Kere J, Carpén O: Myotilin, a novel sarcomeric protein with two Ig-like domains, is encoded by a candidate gene for limb-girdle muscular dystrophy. Hum Mol Genet 1999, 8:1329–1336
5. Parast MM, Otey CA: Characterization of palladin, a novel protein localized to stress fibers and cell adhesions. J Cell Biol 2000, 150: 643–656
6. Mykkänen OM, Grönholm M, Rönty M, Lalowski M, Salmikangas P, Suila H, Carpén O: Characterization of human palladin, a microfilament-associated protein. Mol Biol Cell 2001, 12:3060–3073
7. Bang ML, Mudry RE, McElhinny AS, Trombitas K, Geach AJ, Yamasaki R, Sorimachi H, Granzier H, Gregorio CC, Labeit S: Myopalladin, a novel 145-kilodalton sarcomeric protein with multiple roles in Z-disc and I-band protein assemblies. J Cell Biol 2001, 153:413–427
8. Faulkner G, Lanfranchi G, Valle G: Telethonin and other new proteins of the Z-disc of skeletal muscle. IUBMB Life 2001, 51:275–282
9. Frank D, Kuhn C, Katus HA, Frey N: The sarcomeric Z-disc: a nodal point in signalling and disease. J Mol Med (Berl) 2006, 84:446–468
10. van der Ven PF, Wiesner S, Salmikangas P, Auerbach D, Himmel M, Kempa S, Hayess K, Pacholsky D, Taivainen A, Schröder R, Carpén O, Fürst DO: Indications for a novel muscular dystrophy pathway. gamma-Filamin, the muscle-specific filamin isoform, interacts with myotilin. J Cell Biol 2000, 151:235–248
11. Gontier Y, Taivainen A, Fontao L, Sonnenberg A, van der Flier A, Carpen O, Faulkner G, Borradori L: The Z-disc proteins myotilin and FATZ-1 interact with each other and are connected to the sarcolemma via muscle-specific filamins. J Cell Sci 2005, 118:3739–3749
12. von Nandelstadh P, Ismail M, Gardin C, Suila H, Zara I, Belgrano A, Valle G, Carpen O, Faulkner G: A class III PDZ binding motif in the myotilin and FATZ families binds enigma family proteins: a common link for Z-disc myopathies. Mol Cell Biol 2009, 29:822–834
13. Witt SH, Granzier H, Witt CC, Labeit S: MURF-1 and MURF-2 target a specific subset of myofibrillar proteins redundantly: towards understanding MURF-dependent muscle ubiquitination. J Mol Biol 2005, 350:713–722
14. Salmikangas P, van der Ven PF, Lalowski M, Taivainen A, Zhao F, Suila H, Schröder R, Lappalainen P, Fürst DO, Carpén O: Myotilin, the limb-girdle muscular dystrophy 1A (LGMD1A) protein, cross-links actin filaments and controls sarcomere assembly. Hum Mol Genet 2003, 12:189–203
15. von Nandelstadh P, Grönholm M, Moza M, Lamberg A, Savilahti H, Carpén O: Actin-organising properties of the muscular dystrophy protein myotilin. Exp Cell Res 2005, 310:131–139
16. Selcen D: Myofibrillar myopathies. Curr Opin Neurol 2008, 21:585–589
17. Olivé M, Goldfarb LG, Shatunov A, Fischer D, Ferrer I: Myotilinopathy: refining the clinical and myopathological phenotype. Brain 2005, 128:2315–2326
18. Foroud T, Pankratz N, Batchman AP, Pauciulo MW, Vidal R, Miravalle L, Goebel HH, Cushman LJ, Azzarelli B, Horak H, Farlow M, Nichols WC: A mutation in myotilin causes spheroid body myopathy. Neurology 2005, 65:1936–1940
19. Hauser MA, Conde CB, Kowaljow V, Zeppa G, Taratuto AL, Torian UM, Vance J, Pericak-Vance MA, Speer MC, Rosa AL: Myotilin mutation found in second pedigree with LGMD1A. Am J Hum Genet 2002, 71:1428–1432
20. Hauser MA, Horrigan SK, Salmikangas P, Torian UM, Viles KD, Dancel R, Tim RW, Taivainen A, Bartoloni L, Gilchrist JM, Stajich JM, Gaskell PC, Gilbert JR, Vance JM, Pericak-Vance MA, Carpen O, Westbrook CA, Speer MC: Myotilin is mutated in limb girdle muscular dystrophy 1A. Hum Mol Genet 2000, 9:2141–2147
21. Penisson-Besnier I, Talvinen K, Dumez C, Vihola A, Dubas F, Fardeau M, Hackman P, Carpen O, Udd B: Myotilinopathy in a family with late onset myopathy. Neuromuscul Disord 2006, 16:427–431
22. Berciano J, Gallardo E, Dominguez-Perles R, Garcia A, Garcia-Barredo R, Combarros O, Infante J, Illa I: Autosomal-dominant distal myopathy with a myotilin S55F mutation: sorting out the phenotype. J Neurol Neurosurg Psychiatry 2008, 79:205–208
23. Shalaby S, Mitsuhashi H, Matsuda C, Minami N, Noguchi S, Nonaka I, Nishino I, Hayashi YK: Defective myotilin homodimerization caused by a novel mutation in MYOT exon 9 in the first Japanese limb girdle muscular dystrophy 1A patient. J Neuropathol Exp Neurol 2009, 68:701–707
24. Reilich P, Krause S, Schramm N, Klutzny U, Bulst S, Zehetmayer B, Schneiderat P, Walter MC, Schoser B, Lochmüller H: A novel mutation in the myotilin gene (MYOT) causes a severe form of limb girdle muscular dystrophy 1A (LGMD1A). J Neurol 2011, 258:1437–1444
25. Mavroidis M, Panagopoulou P, Kostavasili I, Weisleder N, Capetanaki Y: A missense mutation in desmin tail domain linked to human dilated cardiomyopathy promotes cleavage of the head domain and abolishes its Z-disc localization. FASEB J 2008, 22:3318–3327
26. Wang X, Osinska H, Klevitsky R, Gerdes AM, Nieman M, Lorenz J, Hewett T, Robbins J: Expression of R120G-alphaB-crystallin causes aberrant desmin and alphaB-crystallin aggregation and cardiomyopathy in mice. Circ Res 2001, 89:84–91
27. Wang X, Osinska H, Dorn GW 2nd, Nieman M, Lorenz JN, Gerdes AM, Witt S, Kimball T, Gulick J, Robbins J: Mouse model of desmin-related cardiomyopathy. Circulation 2001, 103:2402–2407
28. Garvey SM, Miller SE, Claflin DR, Faulkner JA, Hauser MA: Transgenic mice expressing the myotilin T57I mutation unite the pathology associated with LGMD1A and MFM. Hum Mol Genet 2006, 15:2348–2362
29. Hayashi YK, Matsuda C, Ogawa M, Goto K, Tominaga K, Mitsuhashi S, Park YE, Nonaka I, Hino-Fukuyo N, Haginoya K, Sugano H, Nishino I: Human PTRF mutations cause secondary deficiency of caveolins resulting in muscular dystrophy with generalized lipodystrophy. J Clin Invest 2009, 119:2623–2633
30. Thompson TG, Chan YM, Hack AA, Brosius M, Rajala M, Lidov HG, McNally EM, Watkins S, Kunkel LM: Filamin 2 (FLN2): A muscle-specific sarcoglycan interacting protein. J Cell Biol 2000, 148:115–126
31. Schröder R, Schoser B: Myofibrillar myopathies: a clinical and myopathological guide. Brain Pathol 2009, 19:483–492
32. Liu J, Chen Q, Huang W, Horak KM, Zheng H, Mestril R, Wang X: Impairment of the ubiquitin-proteasome system in desminopathy mouse hearts. FASEB J 2006, 20:362–364
33. Liu J, Tang M, Mestril R, Wang X: Aberrant protein aggregation is essential for a mutant desmin to impair the proteolytic function of the ubiquitin-proteasome system in cardiomyocytes. J Mol Cell Cardiol 2006, 40:451–454
34. Selcen D, Ohno K, Engel AG: Myofibrillar myopathy: clinical, morphological and genetic studies in 63 patients. Brain 2004, 127:439–451

35. Claeys KG, Fardeau M, Schröder R, Suominen T, Tolksdorf K, Behin A, Dubourg O, Eymard B, Maisonobe T, Stojkovic T, Faulkner G, Richard P, Vicart P, Udd B, Voit T, Stoltenburg G: Electron microscopy in myofibrillar myopathies reveals clues to the mutated gene. Neuromuscul Disord 2008, 18:656–666
36. Claeys KG, van der Ven PF, Behin A, Stojkovic T, Eymard B, Dubourg O, Laforêt P, Faulkner G, Richard P, Vicart P, Romero NB, Stoltenburg G, Udd B, Fardeau M, Voit T, Fürst DO: Differential involvement of sarcomeric proteins in myofibrillar myopathies: a morphological and immunohistochemical study. Acta Neuropathol 2009, 117:293–307
37. Olivé M: Extralysosomal protein degradation in myofibrillar myopathies. Brain Pathol 2009, 19:507–515
38. Janué A, Olivé M, Ferrer I: Oxidative stress in desminopathies and myotilinopathies: a link between oxidative damage and abnormal protein aggregation. Brain Pathol 2007, 17:377–388
39. Fink AL: Protein aggregation: folding aggregates, inclusion bodies and amyloid. Fold Des 1998, 3:R9–R23
40. Kopito RR: Aggresomes, inclusion bodies and protein aggregation. Trends Cell Biol 2000, 10:524–530
41. Ross CA, Poirier MA: Protein aggregation and neurodegenerative disease. Nat Med 2004, 10:S10–S17
42. von Nandelstadh P, Soliymani R, Baumann M, Carpen O: Analysis of myotilin turnover provides mechanistic insight into the role of myotilinopathy-causing mutations. Biochem J 2011, 436:113–121
43. Goldfarb LG, Vicart P, Goebel HH, Dalakas MC: Desmin myopathy. Brain 2004, 127:723–734
44. Vicart P, Caron A, Guicheney P, Li Z, Prévost MC, Faure A, Chateau D, Chapon F, Tomé F, Dupret JM, Paulin D, Fardeau M: A missense mutation in the alphaB-crystallin chaperone gene causes a desmin-related myopathy. Nat Genet 1998, 20:92–95
45. Selcen D, Muntoni F, Burton BK, Pegoraro E, Sewry C, Bite AV, Engel AG: Mutation in BAG3 causes severe dominant childhood muscular dystrophy. Ann Neurol 2009, 65:83–89
46. Sharma S, Mücke N, Katus HA, Herrmann H, Bär H: Disease mutations in the "head" domain of the extra-sarcomeric protein desmin distinctly alter its assembly and network-forming properties. J Mol Med (Berl) 2009, 87:1207–1219
47. Bär H, Kostareva A, Sjöberg G, Sejersen T, Katus HA, Herrmann H: Forced expression of desmin and desmin mutants in cultured cells: impact of myopathic missense mutations in the central coiled-coil domain on network formation. Exp Cell Res 2006, 312:1554–1565
48. Bova MP, Yaron O, Huang Q, Ding L, Haley DA, Stewart PL, Horwitz J: Mutation R120G in alphaB-crystallin, which is linked to a desmin-related myopathy, results in an irregular structure and defective chaperone-like function. Proc Natl Acad Sci USA 1999, 96:6137–6142
49. Mologni L, Moza M, Lalowski MM, Carpén O: Characterization of mouse myotilin and its promoter. Biochem Biophys Res Commun 2005, 329:1001–1009

Biochemical and Biophysical Research Communications 423 (2012) 212–217

Contents lists available at SciVerse ScienceDirect

Biochemical and Biophysical Research Communications

journal homepage: www.elsevier.com/locate/ybbrc

Regulation of the alternative splicing of *sarcoplasmic reticulum* Ca^{2+}-*ATPase1* (*SERCA1*) by phorbol 12-myristate 13-acetate (PMA) via a PKC pathway

Yimeng Zhao [a], Michinori Koebis [a], Satoshi Suo [a], Shigeo Ohno [b], Shoichi Ishiura [a,*]

[a] *Department of Life Sciences, Graduate School of Arts and Sciences, The University of Tokyo, 3-8-1 Komaba, Meguro-ku, Tokyo 153-8902, Japan*
[b] *Department of Molecular Biology, Yokohama City University Graduate School of Medical Science, 3-9 Fuku-ura, Kanazawa-ku, Yokohama 236-0004, Japan*

ARTICLE INFO

Article history:
Received 6 May 2012
Available online 15 May 2012

Keywords:
Myotonic dystrophy
Sarcoplasmic/endoplasmic reticulum
Ca^{2+}-ATPase 1 (SERCA1)
Alternative splicing
PKC
Phorbol 12-myristate 13-acetate (PMA)
CUG-binding protein 1 (CUGBP1)

ABSTRACT

Myotonic dystrophy type 1 (DM1) is a multi-systemic disease with no established treatment to date. Small, cell-permeable molecules hold the potential to treat DM1. In this study, we investigated the association between protein kinase C (PKC) signaling and splicing of *sarcoplasmic reticulum* Ca^{2+}-*ATPase1* (*SERCA1*). Our aim was to clarify the mechanisms underlying the regulation of alternative splicing, in order to explore new therapeutic strategies for DM1. By assessing the splicing pattern of the endogenous *SERCA1* gene in HEK293 cells, we found that treatment with phorbol 12-myristate 13-acetate (PMA) regulated *SERCA1* splicing. Interestingly, treatment with PMA for 48 h normalized *SERCA1* splicing, while treatment for 1.5 h promoted aberrant splicing. These two responses showed dose dependency and were completely abolished by the PKC inhibitor Ro 31-8220. Furthermore, repression of PKCβII and PKCθ by RNAi mimicked prolonged PMA treatment. These results indicate that PKC signaling is involved in the splicing of *SERCA1* and provide new evidence for a link between alternative splicing and PKC signaling.

1. Introduction

Myotonic dystrophy type 1 (DM1) is an inherited multi-systemic disorder caused by the aberrant expansion of CTG repeats in the *myotonic dystrophy protein kinase* (*DMPK*) 3′-untranslated region (3′-UTR). The clinical presentation of DM1 is highly variable, involving multiple organs, with symptoms including myotonia, cataracts, cardiac conduction defects, progressive muscle wasting and weakness, insulin resistance, and mental retardation. DM1 is a progressive disease; its symptoms become severe with age and across generations.

One reason why aberrantly expanded CTG repeats cause such diverse symptoms is explained by the RNA gain-of-function theory [1]. Expanded CTG repeats are transcribed into RNA with expanded CUG repeats, which possess muscleblind-like protein 1 (MBNL1) binding motifs. MBNL1 is a splicing factor that regulates alternative splicing in several genes (*Clcn1*, *IR*, *cTNT2*, and *SERCA1*) to normalize DM1 splicing abnormalities [2–4]. Ablation of MBNL1 function leads to mis-splicing of several genes. In addition, MBNL1-knockout mice show DM1-like splicing abnormalities and myotonia in their skeletal muscles [5,6]. Moreover, MBNL1-included foci, formed in the nuclei as a result of expanded CUG repeats, were observed by fluorescent immunostaining [3,7]. Thus, levels of free MBNL1 in the cytosol can be decreased by long CUG repeats. Without regulation by MBNL1, the alternative splicing of multiple genes becomes abnormal. Abnormally spliced transcripts are degraded by the nonsense-mediated mRNA decay (NMD) system or translated into abnormal proteins, thereby leading to DM1 symptoms.

Due to the diverse symptoms affecting multiple organs in DM1, its treatment has been limited to supportive care; no basic remedy has been developed. One possible basic remedy is the use of antisense nucleotides to alter the splicing patterns of genes that are aberrantly and indirectly regulated by CUG repeats. However, this method can only treat one gene-derived symptom at a time and requires a great deal of time and effort. Thus, two treatment strategies have been devised: antisense nucleotides against CUG repeats and small molecules. The first strategy uses antisense nucleotides to target CUG repeats and thereby cause repeats to segregate [8], repress [9], or dissolve [10]. However, how to deliver antisense nucleotides into living cells and achieve continual administration remains to be resolved. The other strategy is pharmacological therapy using small molecules. This method can resolve cell permeabilization problems. TG003 has been identified as a compound that improves normal splicing in Duchenne muscular dystrophy (DMD) [11]. In DM1, similarly effective treatment is expected [12,13].

SERCA1 is an aberrantly spliced gene in DM1. SERCA1 protein regulates intracellular Ca^{2+} homeostasis in skeletal muscle cells. The switching of SERCA1 from a fetal isoform, SERCA1b (lacking

Abbreviations: SERCA1, *sarcoplasmic reticulum* Ca^{2+}-*ATPase1*; PMA, phorbol 12-myristate 13-acetate; DM1, myotonic dystrophy type 1; DMPK, myotonic dystrophy protein kinase; MBNL1, muscleblind-like protein 1; CUGBP1, CUG-binding protein 1; CELF, CUG-BP and ETR-3-like (embryonic lethal abnormal vision-type RNA-binding protein 3-like) factor.

* Corresponding author.
E-mail address: cishiura@mail.ecc.u-tokyo.ac.jp (S. Ishiura).

0006-291X/$ - see front matter © 2012 Elsevier Inc. All rights reserved.
http://dx.doi.org/10.1016/j.bbrc.2012.05.033

exon 22), to a mature isoform, SERCA1a (which contains exon 22), is thought to play a central role in muscle development. Since exon 22 contains a stop codon, SERCA1b is six amino acid residues longer than SERCA1a. No specific protein structure has been identified in this six-amino acid residue region [14]. However, in normal skeletal muscle tissues, the expression of *SERCA1a* is strictly regulated [4]; *SERCA1b* is only detected in DM1 patients. Other studies have reported that extended, injured, and fetal muscles express *SERCA1b* [15,16]. Determining the differences between the two isoforms of SERCA1 and their functions is important to our understanding of the DM1 pathogenesis. Expression of *SERCA1b* in DM1 patients indicates that there is some deficiency in this pattern-shift point or in myogenesis. MBNL1 has been identified as a splicing factor that regulates the alternative splicing of *SERCA1* and promotes the production of *SERCA1a* [4]. In this report, we attempted to clarify the mechanisms underlying *SERCA1* splicing to determine the pathogenesis of DM1.

Approximately 500 kinds of protein kinases are involved in signal transduction. Collectively, they regulate diverse cell events, including apoptosis, mitosis, and responses to exogenous stimulators. In the present study, we found that prolonged treatment with phorbol 12-myristate 13-acetate (PMA) normalized *SERCA1* splicing. PMA is a well-known protein kinase C (PKC) activator that imitates diacylglycerol (DAG) and binds to the C1A and C1B domains of PKC isozymes. However, prolonged stimulation with PMA downregulates PKC, thereby inhibiting PKC activation.

PKC regulates various cellular processes including apoptosis, cell division, and cell proliferation. This class of serine/threonine-specific protein kinases can be divided into three groups according to basic structure: conventional PKCs (cPKCs), novel PKCs (nPKCs), and atypical PKCs (aPKCs). The cPKCs (PKCα, PKCβI, PKCβII, and PKCγ contain C1A and C1B domains (DAG binding site) and a C2 domain (Ca^{2+} binding site). The nPKCs (PKCδ, PKCε, PKCη, PKCθ, PKCμ, and PKCν) contain only C1A and C1B domains. The aPKCs (PKCξ and PKCι) have no special DAG or Ca^{2+} binding domains. In the normal state, PKC isozymes are usually inactivated by self-inhibitory effects. cPKC isozymes require Ca^{2+}, DAG, and phosphatidyl serine (PS) for activation, while nPKCs are Ca^{2+}-independent and aPKCs can be activated by PS alone.

The association between DM1 pathogenesis and PKC has been described in two reports. CUG-binding protein 1 (CUGBP1) belongs to the CUG-BP and ETR-3-like (embryonic lethal abnormal vision-type RNA-binding protein 3-like) factor (CELF) family and is one of the key factors inducing aberrant splicing in DM1 (*CLC1*, *cTNT* [17] and *Ca(V)1.1* [18]). It is hyperphosphorylated by CUG repeats and promotes an increase in the steady-state level of CUGBP1. In addition, PKC activation is required for this hyperphosphorylation. Specifically, PKCα and PKCβII have been shown to directly activate CUGBP1 *in vitro* [19]. Furthermore, administration of the PKC inhibitor Ro 31-8220 to DM1 model mice ameliorated cardiac conduction defects in DM1 [20].

In this report, we describe a series of experiments that explored the properties of PKC-mediated alternative splicing using the PKC activator PMA and the PKC inhibitor Ro 31-8220. By exploring the mechanisms regulating the splicing of *SERCA1*, we found that PKCβII and PKCθ were involved in the regulation of *SERCA1* splicing. This report identifies a new regulator of *SERCA1* splicing and a therapeutic strategy for DM1.

2. Materials and methods

2.1. PMA treatment and RT-PCR

HEK293 cells were cultured in Dulbecco's modified Eagle's medium (DMEM) containing 10% fetal bovine serum (FBS) and incubated in an atmosphere containing 5% CO_2 at 37 °C. PMA (final concentration, 5–500 nM) was applied for between 5 min and 48 h. Concentrations of PMA higher than 500 nM induced cell death at 48 h.

Cells were washed with 1 × PBS before cultivation. Total cellular RNA was purified using a GenElute Mammalian Total RNA Miniprep kit (Sigma–Aldrich, MO, USA). Next, 2.5 μg of total RNA was reverse transcribed using a PrimeScript 1st Strand cDNA Synthesis kit (TAKARA BIO, Shiga, Japan) and oligo(dT) primers. *SERCA1* was used to assess the compound's ability to alter splicing patterns. Exons 21 to 23 of endogenous *SERCA1* were amplified by PCR using the following primers: forward, 5′-ATC TTC AAG CTC CGG GCC CT-3′; reverse, 5′-CAG CTC TGC CTG AAG ATG TG) [4]. The annealing temperature was 63.5 °C and there were 30 amplification cycles. PCR products were separated by electrophoresis in an 8% polyacrylamide gel, stained with ethidium bromide, and analyzed using an LAS-3000 luminescence image analyzer (Fujifilm, Tokyo, Japan). Band intensities were digitized and quantified using Multi-gauge (Fujifilm, Tokyo, Japan). Exon 22 inclusion rate (*SERCA1a* percentage) was represented as normal band percentage. Statistical analysis was performed using GraphPad Prism 4 (Graphpad Software, CA, USA).

2.2. RNA interference

For RNAi, siRNAs specific for PKC isozymes except PKCα were designed using BLOCK-iT™ RNAi Designer (Invitrogen, CA, USA). PKCα specific siRNA (SIGMA Genosys, Tokyo, Japan) was designed according to [21]. All siRNA (see sense-strand siRNA sequences in Supplementary Table S1) and negative control RNAi (Stealth™ RNAi Negative Control Low GC Duplex #2) were purchased from Invitrogen and transfected with RNAi MAX (Invitrogen, CA, USA) according to the manufacturer's procedure. Cells were cultured for 48 h after transfection. In the case of PMA treatment, PMA (500 nM) was added to the medium 4 h after transfection.

To verify RNA interference, gene-specific primer sets [22–24] were used to amplify endogenous mRNA. Semi-quantitative RT-PCR or quantitative PCR (see primers and amplification conditions in Supplementary Table S2–S4) was performed. Quantitive PCR was performed with Power SYBR Green PCR Master Mix (Applied BioSystems) using a StepOnePlus™ Real Time PCR System (Applied Biosystems, CA, USA) according to the manufacturer's protocol.

3. Results

3.1. PMA regulates SERCA1 exon 22 splicing

To explore the relationship between PKC and *SERCA1* splicing, we first conducted reverse transcription polymerase chain reaction (RT-PCR) analysis to detect changes in splicing induced by PMA. PMA activates PKC when applied for a short period of time and acts as a PKC downregulator when applied for longer periods of time. As PKC is usually in an inactivated (dephosphorylated) state in cells [25], PMA was considered as an idle compound to explore the regulation of alternative splicing by PKC signaling. We assessed the splicing pattern of endogenous *SERCA1*. *SERCA1a* (3570 bp), which is a normal spliced variant, contains exon 22, while the abnormally spliced variant *SERCA1b* (3528 bp) lacks it. Exons 21–23 of *SERCA1* mRNA were amplified (*SERCA1a*, 240 bp; *SERCA1b*, 198 bp) (Fig. 1A). *SERCA1* is aberrantly spliced in DM1 patients and its splicing pattern is strictly regulated in individuals without DM1. This suggests that regulation of the alternative splicing of *SERCA1* may play a central role in the pathogenesis of DM1. However, the mechanism of *SERCA1* splicing remains to be elucidated.

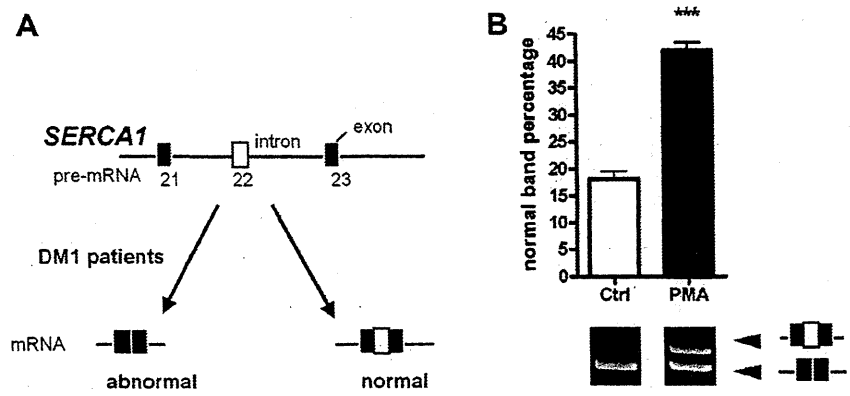

Fig. 1. PMA affects *SERCA1* splicing. (A) Schematic diagram showing two *SERCA1* splicing patterns. (B) RT-PCR analysis of the effects of treatment with 500 nM PMA for 48 h on endogenous *SERCA1* splicing as compared with DMSO (control). Significant differences: ***$P < 0.001$ (Student's *t*-test; mean ± SE; $n = 3$).

Applying 500 nM PMA for 48 h to downregulate PKC in HEK293 cells significantly improved *SERCA1a* splicing (Fig. 1B). It was previously shown that the PKC inhibitor Ro 31-8220 normalized DM1 abnormalities [20], suggesting that downregulation of PKC by PMA led to a change in the *SERCA1* splicing pattern.

3.2. Time-course and dose-curve of PMA effects on SERCA1 exon 22 splicing

To further investigate the signaling pathway involved in the regulation of splicing by PMA, we conducted time-course and dose-curve PMA treatment experiments. Since PKC activation by PMA begins within 5 min [26–29], the time points were set to between 5 min and 72 h (5 min and 0.5, 1.5, 3, 10, 24, 48, and 72 h). After 48 h, normal splicing was increased (Fig. 2A). Promotion of normal splicing continued after 72 h. However, aberrant *SERCA1* splicing was significantly increased after 1.5 h (Fig. 2B). These results indicate dual regulation of alternative splicing of *SERCA1* by PMA.

In the dose-curve analysis, the effects of 5, 50, and 500 PMA were compared with a control (no PMA). The effects of PMA on *SERCA1* splicing at both 1.5 and 48 h were dose-dependent (Fig. 2C and D), supporting the idea that PMA regulates *SERCA1* splicing at both time points. In addition, as 500 nM PMA had the strongest effects on *SERCA1* splicing at both 1.5 and 48 h, subsequent PMA experiments were all conducted with a PMA concentration of 500 nM.

Based on these results, we predicted that PKC plays a critical role in *SERCA1* splicing. We hypothesized that PKC signaling regulates alternative splicing, its activation promotes aberrant splicing of *SERCA1*, and its inhibition or downregulation improves normal splicing of *SERCA1*.

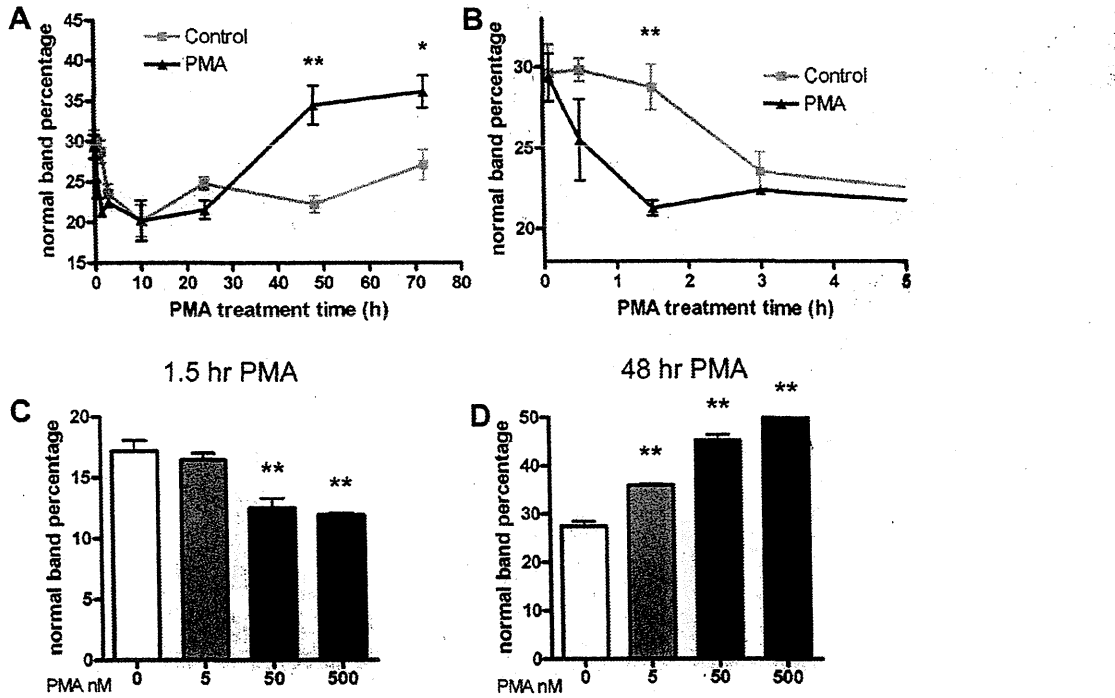

Fig. 2. Regulation of *SERCA1* splicing by PMA. RT-PCR analysis of endogenous *SERCA1* splicing. (A) Time-course of *SERCA1* splicing after stimulation with PMA (500 nM). (B) Data for the first 5 h of the time-course. Controls were treated with DMSO alone. Significant differences: *$P < 0.05$, **$P < 0.01$ (Student's *t* test; mean ± SE; $n = 3$). Dose-curve for the effect of PMA on *SERCA1* splicing (C and D). RT-PCR analysis of normally spliced endogenous *SERCA1* levels in HEK293 cells treated with 0 nM PMA (control) or 5, 50, or 500 nM PMA for 1.5 h (C) or 48 h (D). Significant differences: **$P < 0.01$ (Dunnett's test; mean ± SE; $n = 3$).

3.3. PKC regulates SERCA1 exon 22 splicing

To confirm the involvement of PKC signaling in the response to PMA treatment, the effects of co-treatment with PMA and the PKC inhibitor Ro 31-8220 were examined. Concurrent treatment with Ro 31-8220 (1 μM) completely abolished the effect of PMA treatment (500 nM) for 1.5 h; the level of normally spliced *SERCA1* was upregulated to the same level as in the control (Fig. 3A). Treatment with Ro 31-8220 alone promoted normal *SERCA1* splicing. The effect of PMA (500 nM) at 48 h was completely blocked by Ro 31-8220 (1 μM) (Fig. 3B). Based on these results, we conclude that downregulation of PKC leads to the promotion of *SERCA1a* splicing at 48 h. As 12 PKC isozymes with different functions in different signal transduction pathways have been identified to date, we hypothesized that one or more specific PKC isozymes are involved in the regulation of *SERCA1* splicing.

3.4. Suppression of PKCβII and PKCθ improves SERCA1a splicing

PMA normalizes *SERCA1* splicing, but multiple PKCs (cPKCs and nPKCs) with DAG binding motifs (C1A and C1B sites) can be activated or downregulated (after prolonged stimulation) by PMA. Hence, conventional and novel PKC isozymes may be involved in the regulatory effect of PMA on *SERCA1* splicing. Since aPKCs do not respond to DAG, they can be excluded as candidates. We sought to determine which of the cPKC or nPKC isozymes respond to treatment with PMA for 48 h and improve the production of normal *SERCA1* transcripts. Using RNA interference, we selectively suppressed PKC isozymes and determined whether knockdown of specific isozymes could mimic prolonged PMA stimulation (Fig. 4). Suppression of PKCβII and PKCθ increased normal *SERCA1* splicing, similar to stimulation with PMA for 48 h, while suppression of other PKC isozymes did not affect *SERCA1* splicing. Based on these results, we conclude that depletion of PKCβII and PKCθ improves *SERCA1a* splicing in HEK293 cells.

4. Discussion

In this study, we clarified the mechanism underlying PKC-mediated regulation of *SERCA1* splicing abnormalities in DM1. First, we identified PMA, a widely-used PKC activator and downregulator of PKC during prolonged stimulation, as a compound that effectively normalizes *SERCA1* splicing in HEK293 cells. By examining the properties of PMA's regulatory effects on *SERCA1* splicing, we found that PMA improved normal splicing during treatment for 48 h, while it increased aberrant splicing at 1.5 h. Two peaks for the effects of PMA on *SERCA1* splicing were confirmed to be dose-dependent. We then attempted to determine whether PKC is involved in PMA stimulation using the PKC inhibitor Ro 31-8220. Ro 31-8220 abolished the effects of PMA at both 1.5 and 48 h. However, treatment with Ro 31-8220 alone for 48 h did not affect splicing at all. This may be due to self-inhibition of PKC, meaning that Ro 31-8220 could not inhibit PKC, leaving *SERCA1* splicing unchanged. We thus confirmed the involvement of PKC in the regulation of *SERCA1* splicing by PMA.

The alternative splicing of several genes, including *Bcl-x*, *Axl* [30], and *CD45* [31], has have been reported to be affected by PKC-mediated phosphorylation. In addition, the connection between PKC and splicing-related factors (PSF, hnRNP A3, p68 RNA helicase, and hnRNP L) supports the idea that PKC regulates alternative splicing [32]. However, no specific PKC isozyme has been identified as a splicing regulator.

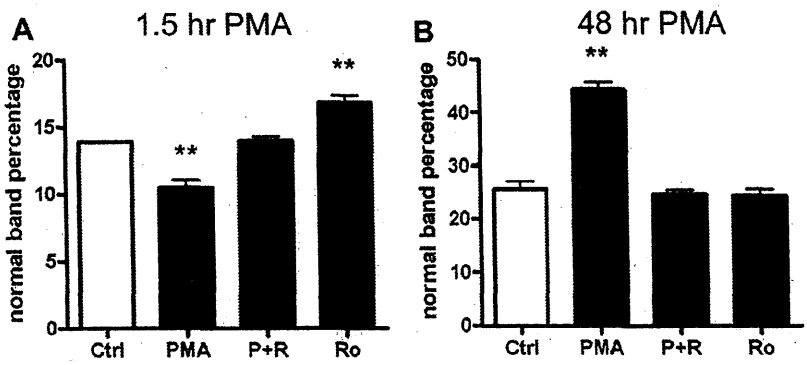

Fig. 3. PMA regulates *SERCA1* splicing via a PKC pathway. RT-PCR analysis of endogenous *SERCA1* splicing in HEK293 cells. PMA and the PKC inhibitor Ro 31-8220 were co-administered for 1.5 h (A) or 48 h (B). Controls were treated with DMSO alone. P = PMA (500 nM); R, Ro = Ro 31-8220 (1 μM). Significant differences: $^{**}P < 0.01$ (Dunnett's test; mean ± SE; $n = 3$).

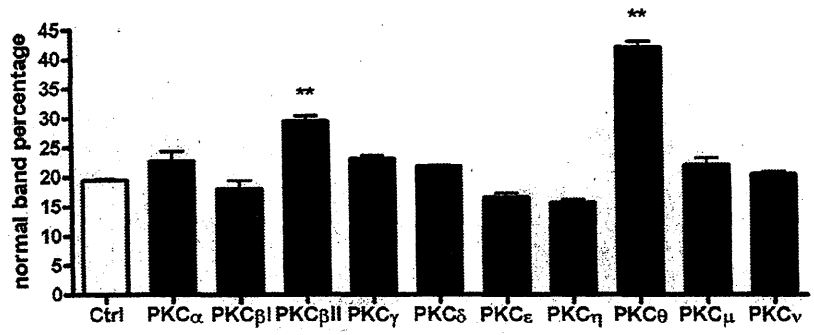

Fig. 4. RNA interference of PKC isozymes mimicked PMA regulation of *SERCA1* splicing. RT-PCR analysis of normally spliced endogenous *SERCA1* in HEK293 cells. RNAi specific for PKC isozymes (PKCα, PKCβI, PKCβII, PKCγ, PKCδ, PKCε, PKCη, PKCθ, PKCμ, or PKCν) as compared with control siRNA. Significant differences: $^{**}P < 0.01$ (Dunnett's test; mean ± SE; $n = 3$).

PKC is known to be involved in many diseases, including cancer, Alzheimer's disease, autoimmune diseases, and cardiovascular diseases. The association between the pathogenesis of DM1 and PKC was mentioned in previous reports [19,20], and CUGBP1 is the key to this association. Hyperphosphorylation of CUGBP1 has been confirmed in DM1 tissues, cells, and model mice and promotes an increase in the steady-state levels of CUGBP1. PKC activation is required for this hyperphosphorylation. Specifically, PKCα and PKCβII have been shown to directly activate CUGBP1 *in vitro* [19]. Furthermore, administration of the PKC inhibitor Ro 31-8220 to DM1 model mice ameliorated cardiac conduction defects [20]. These reports are consistent with our finding that PMA regulates the alternative splicing of *SERCA1* via a PKC pathway.

By selectively reducing the expression of PKC isozymes with siRNA, we identified PKCβII and PKCθ as isozymes that mimic 48 h PMA treatment. These two PKC isozymes promote production of the aberrant isoform *SERCA1b*. PKCθ is mainly expressed in skeletal muscle and T cells, which suggests that it plays crucial roles in myogenesis and the immune system [33,34]. Very recently, abolishing PKCθ in *mdx* (DMD model) mice was shown to prevent muscle wasting and improve muscle regeneration, maintenance, and performance [35]. DMD and DM1 are both progressive muscular dystrophies that have multiple symptoms in common (muscle weakness and muscular atrophy). Similar to DMD, our results showing that reductions in endogenous PKCθ levels in HEK293 cells induced normal *SERCA1* splicing in DM1 suggest that PKCθ is a candidate pharmacological therapeutic target in DM1. PKCβII, a Ca^{2+}-dependent isozyme, was shown to be involved in PMA-mediated CUGBP1 hyperphosphorylation, which induced DM1-like splicing abnormalities in a previous study[20]. So, we hypothesize that CUGBP1 may respond to PMA-induced PKC signaling. Interestingly, however, there were two discrepancies in the response of CUGBP1 to PKC signaling in the regulation of *SERCA1* splicing. First, CUGBP1 was previously shown to have no direct effect on *SERCA1* splicing [4], as demonstrated by overexpression of CUGBP1 in HEK293 cells and deduced from the observation of altered splicing of the *SERCA1* minigene and of endogenous *SERCA1* in C2C12 primary murine myoblast cells. The other difference is that CUGBP1 hyperphosphorylation peaks 3 h after PMA treatment [19]. This is 1.5 h after our *SERCA1* splicing pattern. We are going to check this issue by multiple methods: silencing endogenous CUGBP1 expression and overexpress recombinant CUGBP1, or other CELF families. Unfortunately, the slight but significant effect of stimulation with PMA for 1.5 h prevented us from identifying the PKC isozymes that respond to treatment with PMA for 1.5 h using siRNA.

To summarize, this is the first report to show that PKCβII and PKCθ are involved in the regulation of *SERCA1* alternative splicing. Note that PKCθ has not been reported to be involved in the regulation of alternative splicing. These findings suggest the existence of a neo-alternative splicing regulation pathway that operates via PKC. In conclusion, we not only identified novel potential therapeutic targets for DM1 treatment, but also showed the existence of a new alternative splicing regulatory mechanism.

Acknowledgments

We thank Drs. Y. Kino, K. Kanno, and Y. Nagara for valuable discussions. This work was supported by intramural research Grants (23-5) for Neurological and Psychiatric Disorders from the NCNP, Ministry of Health, Labour and Welfare, Japan.

Appendix A. Supplementary data

Supplementary data associated with this article can be found, in the online version, at http://dx.doi.org/10.1016/j.bbrc.2012.05.033.

References

[1] L.P. Ranum, J.W. Day, Myotonic dystrophy: RNA pathogenesis comes into focus, Am. J. Hum. Genet. 74 (2004) 793–804.
[2] A. Mankodi, M.P. Takahashi, H. Jiang, et al., Expanded CUG repeats trigger aberrant splicing of ClC-1 chloride channel pre-mRNA and hyperexcitability of skeletal muscle in myotonic dystrophy, Mol. Cell 10 (2002) 35–44.
[3] T.H. Ho, B.N. Charlet, M.G. Poulos, et al., Muscleblind proteins regulate alternative splicing, EMBO J. 23 (2004) 3103–3112.
[4] S. Hino, S. Kondo, H. Sekiya, et al., Molecular mechanisms responsible for aberrant splicing of SERCA1 in myotonic dystrophy type 1, Hum. Mol. Genet. 16 (2007) 2834–2843.
[5] R.N. Kanadia, K.A. Johnstone, A. Mankodi, et al., A muscleblind knockout model for myotonic dystrophy, Science 302 (2003) 1978–1980.
[6] M. Hao, K. Akrami, K. Wei, et al., Muscleblind-like 2 (Mbnl2) -deficient mice as a model for myotonic dystrophy, Dev. Dyn. 237 (2008) 403–410.
[7] A. Mykowska, K. Sobczak, M. Wojciechowska, et al., CAG repeats mimic CUG repeats in the misregulation of alternative splicing, Nucleic Acids Res. 39 (2011) 8938–8951.
[8] T.M. Wheeler, K. Sobczak, J.D. Lueck, et al., Thornton, Reversal of RNA dominance by displacement of protein sequestered on triplet repeat RNA, Science 325 (2009) 336–339.
[9] S.A. Mulders, W.J. van den Broek, T.M. Wheeler, et al., Triplet-repeat oligonucleotide-mediated reversal of RNA toxicity in myotonic dystrophy, Proc. Nat. Acad. Sci. U.S.A 106 (2009) 13915–13920.
[10] J. Kurreck, Antisense technologies. Improvement through novel chemical modifications, Eur. J. Biochem. 270 (2003) 1628–1644.
[11] A. Nishida, N. Kataoka, Y. Takeshima, et al., Chemical treatment enhances skipping of a mutated exon in the dystrophin gene, Nat. Commun. 2 (2011) 308, http://dx.doi.org/10.1038/ncomms1306.
[12] D.A. O'Leary, L. Vargas, O. Sharif, et al., HTS-compatible patient-derived cell-based assay to identify small molecule modulators of aberrant splicing in myotonic dystrophy type 1, Curr. Chem. Genomics 4 (2010) 9–18.
[13] E.L. Logigian, W.B. Martens, R.T. Moxley IV, et al., Mexiletine is an effective antimyotonia treatment in myotonic dystrophy type 1, Neurology 74 (2010) 1441–1448.
[14] C. Toyoshima, M. Nakasako, H. Nomura, et al., Crystal structure of the calcium pump of sarcoplasmic reticulum at 2.6 A resolution, Nature 405 (2000) 647–655.
[15] E. Zádor, L. Mendler, M. Ver Heyen, et al., Changes in mRNA levels of the sarcoplasmic/endoplasmic-reticulum Ca(2+)-ATPase isoforms in the rat soleus muscle regenerating from notexin-induced necrosis, Biochem. J. 320 (1996) 107–113.
[16] E. Zádor, L. Dux, F. Wuytack, Prolonged passive stretch of rat soleus muscle provokes an increase in the mRNA levels of the muscle regulatory factors distributed along the entire length of the fibers, J. Muscle Res. Cell Motil. 20 (1999) 395–402.
[17] T.H. Ho, D. Bundman, D.L. Armstrong, et al., Transgenic mice expressing CUG-BP1 reproduce splicing mis-regulation observed in myotonic dystrophy, Hum. Mol. Genet. 14 (2005) 1539–1547.
[18] Z.Z. Tang, V. Yarotskyy, L. Wei, et al., Muscle weakness in myotonic dystrophy associated with misregulated splicing and altered gating of CaV1.1 calcium channel, Hum. Mol. Genet. 21 (2012) 1312–1324.
[19] N.M. Kuyumcu-Martinez, G.S. Wang, T.A. Cooper, Increased steady-state levels of CUGBP1 in myotonic dystrophy 1 are due to PKC-mediated hyperphosphorylation, Molecular Cell 28 (2007) 68–78.
[20] G.S. Wang, M.N. Kuyumcu-Martinez, S. Sarma, et al., PKC inhibition ameliorates the cardiac phenotype in a mouse model of myotonic dystrophy type 1, J. Clin. Invest. 119 (2009) 3797–3806.
[21] N. Irie, N. Sakai, T. Ueyama, et al., Subtype- and species-specific knockdown of PKC using short interfering RNA, Biochem. Biophys. Res. Commun. 298 (2002) 738–743.
[22] H. Sakai, M. Yamamoto, Y. Kozutsumi, et al., Identification of PKC isoforms expressed in human bronchial smooth muscle cell, J. Smooth Muscle Res. 45 (2009) 55–62.
[23] K.I. Nagata, Y. Okano, Y. Nozawa, Protein kinase C isozymes in human megakaryoblastic leukemia cell line, MEG-01: possible involvement of the isozymes in the differentiation process of MEG-01 cells, Br. J. Haematol. 93 (1996) 762–771.
[24] A. Hayashi, N. Seki, A. Hattori, et al., PKCnu, a new member of the protein kinase C family, composes a fourth subfamily with PKCmu, Biochim. Biophys. Acta. 1450 (1999) 99–106.
[25] J.W. Orr, A.C. Newton, Intrapeptide regulation of protein kinase C, J. Biol. Chem. 269 (1994) 8383–8387.
[26] G. Nowak, Protein kinase C mediates repair of mitochondrial and transport functions after toxicant-induced injury in renal cells, J. Pharmacol Exp. Ther. 306 (2003) 157–165.
[27] M.C. Meyer, P.J. Kell, M.H. Creer, et al., Calcium-independent phospholipase A2 is regulated by a novel protein kinase C in human coronary artery endothelial cells, Am. J. Physiol. Cell Physiol. 288 (2005) C475–C482.
[28] M.H. Disatnik, S.C. Boutet, C.H. Lee, et al., Sequential activation of individual PKC isozymes in integrin-mediated muscle cell spreading: a role for MARCKS in an integrin signaling pathway, J. Cell Sci. 115 (2002) 2151–2163.

[29] A. Di, X.P. Gao, F. Qian, et al., The redox-sensitive cation channel TRPM2 modulates phagocyte ROS production and inflammation, Nat. Immunol. 13 (2011) 29–34.
[30] T. Revil, J. Toutant, L. Shkreta, et al., Protein kinase C-dependent control of Bcl-x alternative splicing, Mol. Cell. Biol. 27 (2007) 8431–8441.
[31] K.W. Lynch, A. Weiss, A model system for activation-induced alternative splicing of CD45 pre-mRNA in T cells implicates protein kinase C and Ras, Mol. Cell Biol. 20 (2000) 70–80.
[32] U. Rosenberger, I. Lehmann, C. Weise, et al., Identification of PSF as a protein kinase Calpha-binding protein in the cell nucleus, J. Cell Biochem. 86 (2002) 394–402.
[33] S. Osada, K. Mizuno, T.C. Saido, et al., A new member of the protein kinase C family, nPKCθ, predominantly expressed in skeletal muscle, Mol. Cell Biol. 12 (1992) 3930–3938.
[34] G. Baier, D. Telford, L. Giampa, et al., Molecular cloning and characterization of PKCθ, a novel member of the protein kinase C (PKC) gene family expressed predominantly in hematopoietic cells, J. Biol. Chem. 268 (1993) 4997–5004.
[35] L. Madaro, A. Pelle, C. Nicoletti, et al., PKC theta ablation improves healing in a mouse model of muscular dystrophy, PLoS One 7 (2012) e31515, http://dx.doi.org/10.1371/journal.pone.0031515.